Environment International 183 (2024) 108252

Contents lists available at ScienceDirect

Environment International

journal homepage: www.elsevier.com/locate/envint

Full length article

Uncertainties in source allocation of carbonaceous aerosols in a Mediterranean region

Hector Navarro-Barboza [a,*], Marco Pandolfi [b], Marc Guevara [a], Santiago Enciso [a,1], Carles Tena [a], Marta Via [b], Jesus Yus-Díez [b,2], Cristina Reche [b], Noemi Pérez [b], Andrés Alastuey [b], Xavier Querol [b], Oriol Jorba [a]

[a] Barcelona Supercomputing Center, Plaça Eusebi Güell 1-3, Barcelona 08034, Spain
[b] Institute of Environmental Assessment and Water Research, c/Jordi-Girona 18-26, Barcelona 08034, Spain

ARTICLE INFO

Handling Editor: Marti Nadal

ABSTRACT

Understanding the atmospheric processes involving carbonaceous aerosols (CAs) is crucial for assessing air pollution impacts on human health and climate. The sources and formation mechanisms of CAs are not well understood, making it challenging to quantify impacts in models. Studies suggest residential wood combustion (RWC) and traffic significantly contribute to CAs in Europe's urban and rural areas.

Here, we used an atmospheric chemistry model (MONARCH) and three different emission inventories (two versions of the European-scale emission inventory CAMS-REG_v4 and the HERMESv3 detailed national inventory for Spain) to assess the uncertainties in CAs simulation and source allocation (from traffic, RWC, shipping, fires and others) in Northeast Spain. For this, black carbon (BC) and organic aerosol (OA) measurements performed at three supersites representing different environments (urban, regional and remote) were used. Our findings show the importance of model resolution and detailed emission input data in accurately reproducing BC/OA observations. Even though emissions of total particulate matter are rather consistent between inventories in Spain, we found discrepancies between them mainly related to the spatiotemporal disaggregation (particularly relevant for traffic and RWC) and the treatment of the condensable fraction of CAs in RWC (changes in the speciation of elemental/organic carbon). The main source contribution to BC concentrations in the urban site is traffic, accounting for 71.1%/65.2% (January/July) in close agreement with the fossil contribution derived from observations (78.8%/84.2%), followed by RWC (12.8%/3%) and shipping emissions (5.4%/13.8%). An overrepresentation of RWC (winter) and shipping (summer) is obtained with CAMS-REG_v4. Noteworthy uncertainties arise in OA results due to condensables in emissions and a limited secondary aerosol production in the model.

These findings offer insights into MONARCH's effectiveness in simulating CAs concentrations and source contribution in Northeast Spain. The study highlights the benefits of combining new datasets and modeling techniques to refine emission inventories and better understand and mitigate air pollution impacts.

1. Introduction

According to the World Health Organization (WHO), 91% of the global population was exposed to polluted air resulting in 4.2 million premature deaths in both urban and rural areas worldwide in 2016 (WHO, 2018). Numerous studies have directly linked exposure to polluted environments with pulmonary and cardiovascular diseases (e.g., Poloniecki et al., 1997; Schwartz, 2000; Bell et al., 2006; Tie et al., 2009; Foster and Kumar, 2011; Chen et al., 2018; Yue et al., 2023). Fine and ultrafine particles are considered one of the most harmful air pollutants due to their ability to be absorbed by lung cells (Kennedy, 2007; Ohlwein et al., 2019; Moreno-Ríos et al., 2022). Despite the reduction in the emission of harmful substances in the last decades, the number of premature deaths remains high in Europe (EEA, 2022). Improving air

* Corresponding author.
E-mail address: hector.navarro@bsc.es (H. Navarro-Barboza).
[1] Now at Applus IDIADA Group, Tarragona, Spain.
[2] Now at Centre for Atmospheric Research, University of Nova Gorica, Vipavska 11c, SI-5270 Ajdovščina, Slovenia.

https://doi.org/10.1016/j.envint.2023.108252
Received 21 May 2023; Received in revised form 4 October 2023; Accepted 5 October 2023
Available online 17 October 2023

quality will require significant efforts to reduce emissions from several activity sectors (e.g. transport, industrial or household sources). Carbonaceous aerosols (CAs) includes a fraction of organic aerosols (OA), or organic matter (OM) and a refractory light-absorbing component referred to as black carbon (BC) or elemental carbon (EC). CAs are predominantly present in the fine size fraction of particulate matter (Echalar et al., 1998; Hitzenberger and Tohno, 2001) and strongly impact climate, air pollution, human health, and ecosystems. The emissions of CAs are attributed partly to incomplete combustion of fossil fuel, coal or biomass burning. Both traffic and residential wood combustion (RWC) are important sources to CAs (Chen et al., 2022). In Europe, around 50% of the total anthropogenic $PM_{2.5}$ emissions are estimated to be CAs and the main source of primary OA is attributed to RWC (Denier Van Der Gon et al., 2015). Several field studies have shown the large fraction of OA in the chemical composition of $PM_{2.5}$ concentrations (e.g., Jimenez et al., 2009). Although European climate policies promote wood burning as a source of energy to meet targeted reductions in carbon emissions (Validzic, 2017), this also has negative consequences for air quality as it generates harmful gases and aerosol particles mainly in the fine fraction (Chafe et al., 2015). A proper understanding of air pollution is critical in the design and implementation of effective policy solutions.

Historically, numerical models have been essential tools for decision-makers in formulating plans to reduce atmospheric pollution. However, simulating CA concentrations with models, particularly during cold seasons, has proven to be challenging (Aas et al., 2012). Multi-model intercomparison studies have shown significant underestimations of particulate organic carbon (OC) and EC concentrations over Europe in the fine fraction of PM by 40 −80% and 20 −60%, respectively (Prank et al., 2016). Models have difficulty simulating the secondary organic aerosol (SOA) formation because they do not fully represent the atmospheric oxidation processes, resulting in the underestimation of OC concentrations. This is due to the generation of low-volatility organic compounds, which is not well-captured by current models (Hallquist et al., 2009; Shrivastava et al., 2017). Furthermore, the limitation on the representation of CAs in models is also driven by uncertainties in the underlying emission inventories used as input, particularly from inaccuracies related to the inclusion of condensable compounds and reproduction of spatial patterns.

Condensable compounds refer to the portion of material emitted into the atmosphere as gas that rapidly condenses into particulate matter without undergoing chemical reactions (Simpson et al., 2020). The inclusion or exclusion of this condensable fraction in emission inventories is one of the major uncertainties regarding CAs combustion sources, mainly due to the particulate matter measurement techniques used to derive emission factors. Nussbaumer et al. (2008) outlines various sampling methods and their respective emission factors, with the most crucial ones being filter measurements, which only measure solid particles (SP), and dilution tunnel (DT) measurements, which measure solid particles and condensable or semi-volatile organics. The choice of SP or DT emission factors can lead to significant differences, with a fivefold discrepancy in absolute PM emission estimates depending on which one is used (Denier Van Der Gon et al., 2015).

The use of condensable emission factors is currently inconsistent in emission inventories across different sectors, which may lead to underestimations of particulate matter (PM) emissions. For example, emission measurements in the road transport sector include the condensable component, while industrial sources exclude it. Additionally, some approaches include condensable in the emission factors for small-scale combustion of coal or wood, while others do not (Simpson et al., 2020). Denier Van Der Gon et al. (2015) showed that the inclusion of the condensable fraction in the emission inventory for RWC in Europe resulted in substantially improved agreement between measured and predicted OA. Similarly, Morino et al. (2018) highlighted the benefit of considering the fraction of condensable fraction from stationary combustion sources to improve OA model results over Japan during winter. The inclusion of condensable material in emission inventories is a major topic of research for the modelling community. In fact, it is not only crucial if today's emissions inventories include the condensable fraction, but also how these inventories include this fraction and on which sectors (Bergström, 2020).

Uncertainties in the spatial distribution of primary CAs emissions, particularly from burning of wood and coal in the residential sector, have also been highlighted as a major limitation in current emission inventories. Spatial patterns can significantly vary between countries, as suggested by Trombetti et al. (2018). While wood burning is common in rural areas due to limited access to natural gas, there can be also high activity recorded in urban areas due to sociodemographic or economic aspects (Grythe et al., 2019; Athanasopoulou et al., 2017); however, this may not be representative of southern European countries (Timmermans et al., 2013; Kuenen et al., 2022). The development of spatial proxies capable of capturing this heterogeneity between regions is challenging, as it requires the use of very detailed and up-to-date information on household appliances (Paunu et al., 2021). As a consequence, important discrepancies arise when comparing the spatial distribution of RWC emissions as reported by regional and local emission inventories. For instance, the comparison of fine scale bottom-up inventories against three regional inventories (i.e., EC4MACS, TNO-MACC-II and TNO-MACC-III) for seven urban areas in Norway indicated discrepancies in $PM_{2.5}$ emissions from RWC of up 90% (López-Aparicio et al., 2017). Thunis et al. (2021) compared a global inventory (EDGAR, (Crippa et al., 2018)) against two regional inventories (EMEP (Nielsen, 2013), CAMS-REG-AP (Kuenen et al., 2003)) over the European continent and showed that despite the different approaches used in each inventory to estimate emissions, all three led to consistent results for $PM_{2.5}$. However, the main discrepancies between the results were attributed to the spatial variability. The study highlights the importance of complementing validation with observations with other evaluation approaches, such as source apportionment (SA), since overestimates in one sector can offset other sectors. It should be noted however that SA techniques applied to observational CAs data are also prone to potentially high uncertainties in part due to a priori assumptions needed for SA that could not reflect the actual physical properties of CA particles, especially of BC.

In this contribution, we investigate the uncertainties in representing CAs source contribution in the Western Mediterranean basin (WMB) by combining modelling and monitoring techniques. We focus on the contribution of RWC, traffic, shipping, and biomass burning emissions, as well as their spatial characterization, including CAs speciation and treatment of condensable fraction. To achieve this, we employ the Multiscale Online Nonhydrostatic Atmosphere CHemistry model (MONARCH; Badia and Jorba, 2015; Badia et al., 2017; Klose et al., 2021) with different emission inventories and evaluate the results against data from three monitoring supersites representing different environments (urban, regional and remote). The final goal is to provide insights into the contributions of these sectors to CAs concentrations and their impact on air quality.

The structure of the paper is as follows. In Section 2, we describe the region and period of study, as well as the evaluation observational datasets providing information on the mass and source contribution of CAs. We present a detailed description of the atmospheric chemistry model used in this study. We also provide an overview of the different emission inventories employed and the statistical metrics selected for the analysis. In Section 3, we present the results of the work. First, we perform an inter-comparison between different emission inventories over Spain, followed by an analysis of the BC and OA surface concentrations and source contribution model results. Finally, Section 4 provides a summary of the results and the main conclusions.

2. Materials and methods

2.1. Domain and period of study

The study is conducted over the Northeast (NE) region of Spain, located in the Western Mediterranean Basin (WMB) (Fig. 1). This area is known for high pollution levels due to a combination of atmospheric dynamics, local orography and various anthropogenic and natural sources. The WMB is home to several large cities, industrial areas, and ports along the coast, which are significant sources of atmospheric particulate matter (PM) and precursor gases (Jorba et al., 2013; Pandolfi et al., 2014). The region is also affected by dust transport from North Africa, which contributes to higher coarse particulate matter (PM) loading in the region, particularly during spring/summer (Querol et al., 2009; Pey et al., 2013). The study focuses on the year 2018 and utilizes observational data from three different environments: urban background, regional background, and remote background. These measurement sites located in NE Spain offer a comprehensive understanding of the physico-chemical properties of atmospheric aerosol particles in the region. During the warm season, a characteristic sea-breeze circulation advects air masses from Barcelona city towards the Montseny environment (Jorba et al., 2013). During cold seasons, the Azores High occasionally shifts south, allowing Atlantic low-pressure systems to enter the Mediterranean. This helps clear stagnant air and reduces pollution at a regional scale (Pandolfi et al., 2014).

2.2. Observational dataset

2.2.1. Measuring sites

We use three atmospheric research supersites run by the Environmental Geochemistry and Atmosphere Group of the Institute of Environmental Analysis and Water Research (EGAR-IDAEA): one located in the city of Barcelona representative of urban background (URB), the second one located in a regional background environment, named Montseny (REG), and the third one located in a remote background environment, named Montsec (REM) (see geographic coordinates and height in Table 1). These measurement stations are characterized by aerosols with different physical and chemical properties. URB is located within the Barcelona metropolitan area of nearly 4.5 million inhabitants at a distance of about 25 km from the coast, and at 200 m distance from one of the busiest streets in the city (> 60 k vehicles per day). REG station is located in a hilly and densely forested area within the Natural Park and Biosphere Reserve of Montseny, 50 km to the N-NE of Barcelona and 25 km from the Mediterranean coast. The REM station is located in a remote high-altitude emplacement on the southern side of the Pre-Pyrenees at the Montsec Range, 140 km to the NW of Barcelona and 140 km to the WNW of REG. These supersites are part of the Catalonian Atmospheric Pollution Monitoring and Forecasting Network and of the ACTRIS (www.actris.eu) and GAW (www.wmo.int) networks. A detailed characterization of these measurement stations can be found in previous works (e.g. Querol et al., 2001; Rodrıguez et al., 2001; Reche et al., 2011; Brines et al., 2014; Ealo et al., 2018 for URB; Pérez et al., 2008; Pey et al., 2009; Pandolfi et al., 2014; Pandolfi et al., 2016 for REG; Ripoll et al., 2014; Ripoll et al., 2015 and Ealo et al., 2016, for REM).

Table 1 summarizes the observations used from each site in this study and Fig. 2 shows their location. In the following sections, we provide a brief description of them. Additionally, the aerosol evaluation is complemented with meteorological observations of air temperature at 2 m and wind speed at 10 m above ground level available at URB and REG sites.

2.2.2. Online BC measurements

BC concentrations were determined with Multi Angle Absorption Photometer (MAAP, Thermo Fisher Scientific, Waltham, USA; Petzold and Schönlinner, 2004) instruments at the three sites (URB, REG and REM).

MAAP is a filter-based method, i.e. the aerosol sample is continuously collected on a filter tape. This instrument derives the absorption coefficient at 637 nm (Müller et al., 2011) using a radiative transfer model from the measurements of transmission of light through the filter tape and backscattering of light at two different angles (Petzold et al., 2005). The eBC concentrations are calculated by the MAAP's software using a mass absorption cross section (MAC) value of 6.6 m^2/g. However, the MAC can vary considerably from one site to another due to its dependency on the BC sources and on the degree of internal mixing of BC particles with other chemical components (e.g., Pandolfi et al., 2011; Zanatta et al., 2016; Yus-Díez et al., 2022). Internal mixing or coating can enhance the absorption efficiency of BC particles, resulting in a higher MAC. This is due to the so-called lensing effect, whereby more photons are focused on the BC core, leading to increased absorption. As a result, determining the local MAC is crucial for accurately measuring BC concentrations using filter absorption photometers like the MAAP. Without accounting for local MAC, measurements can be highly uncertain. Here the more suitable MAC for the three measurement sites (URB, REG and REM) was calculated by comparing the absorption measurements provided by the MAAP with the EC concentrations obtained with a semi-continuous (3 h resolution) SUNSET analyzer in URB (Karanasiou et al., 2020) and a laboratory (24 h time resolution) off-line SUNSET instruments at REG and REM. Both instruments (semi-continuous and off-line) provided EC and OC concentrations using the EUSAAR_2 standard protocol (Cavalli et al., 2010).

The average MAC values used here to estimate the BC concentrations were 9.6 $\pm$ 3.2 m^2/g, 12.5 $\pm$ 3.2 m^2/g and 13.2 $\pm$ 3.2 m^2/g at URB, REG and REM, respectively, as supported by the treatments detailed in Yus-Díez et al. (2022). The MAC values consistently increased from URB

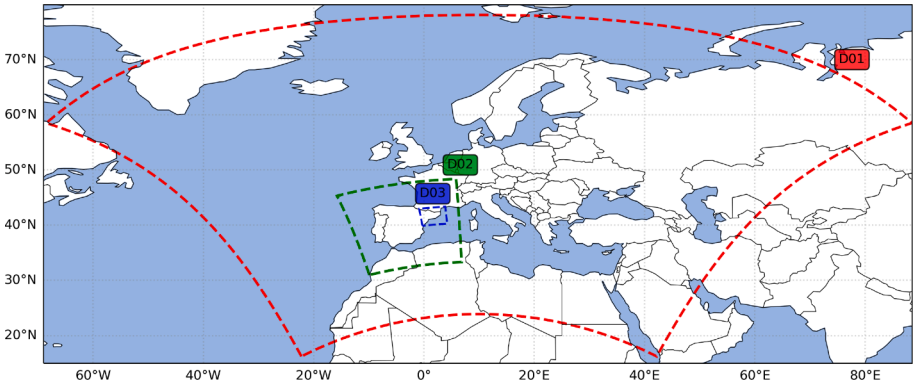

Fig. 1. Domain of study and model nest configuration. D01 parent domain at ~ 20 km horizontal resolution, D02 nest domain at ~ 5 km, and D03 inner domain at ~ 1 km covering NE Spain.

Table 1
Measurements used for the evaluation of the MONARCH model.

Station	Variable	Instrument	Resolution	Size	Coordinates		
					Latitude (N)	Longitude (E)	Altitude
URB	OC/EC	SUNSET analyzer	24 h	$PM_{2.5}$	41°23′24″	02°6′58″	67 ma.s.l.
	OA	ACSM	1 h	PM_1			
	BC/Abs	MAAP/AE33	1 h	PM_{10}			
REG	OC/EC	SUNSET analyzer	24 h	$PM_{2.5}$	41°19′	02°21′	720 ma.s.l.
	BC/Abs	MAAP/AE33	1 h	PM_{10}			
REM	OC/EC	SUNSET analyzer	24 h	PM_{10}	42°3′	0°44′	1570 ma.s.l.
	BC/Abs	MAAP/AE33	1 h	PM_{10}			

a Abs: absorption.

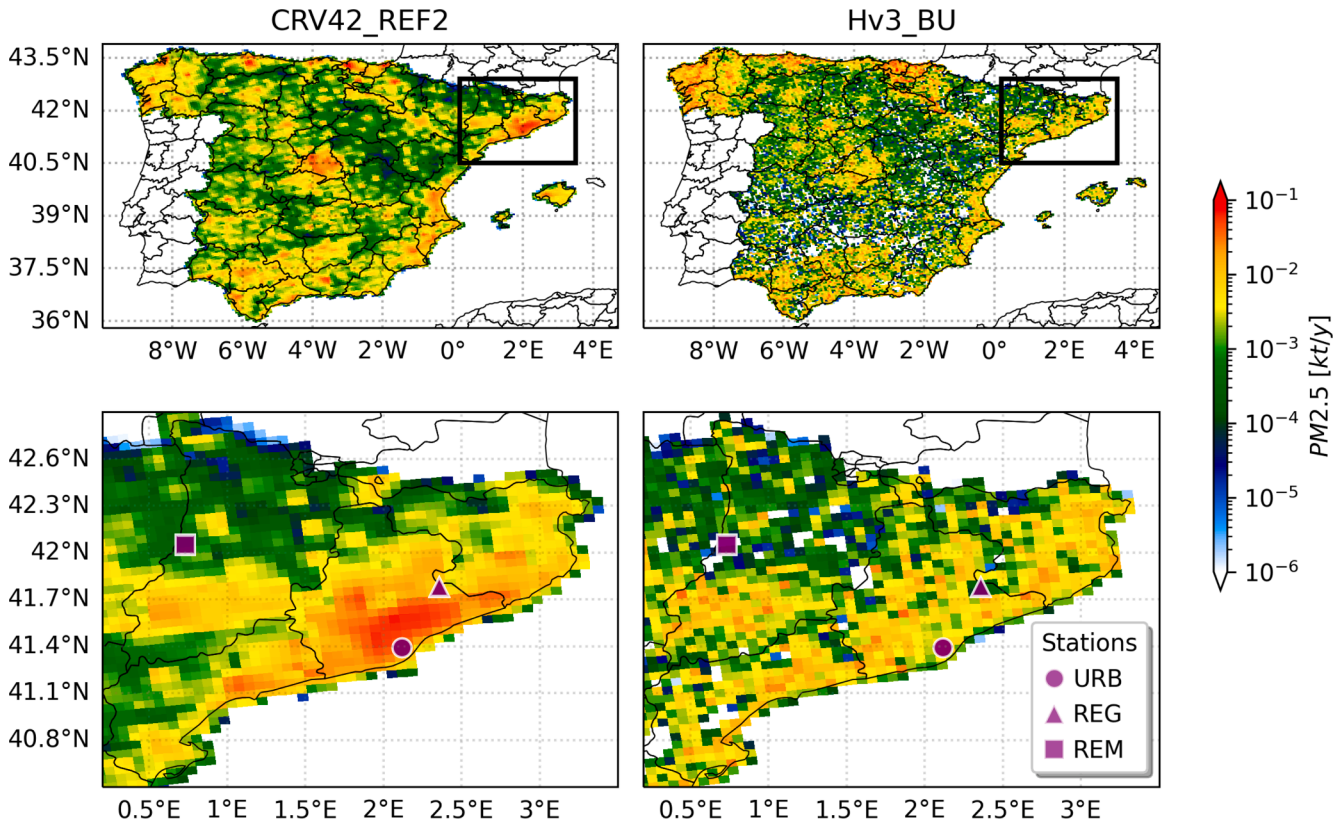

Fig. 2. Annual RWC emissions for Spain from CRV42_REF2 (68.8 kt/y) and Hv3_BU (63.9 kt/y) gridded at 5 km horizontal resolution. Bottom panel shows a zoom in NE Spain. Symbols indicate the localization of the three monitoring sites used in this work.

(urban) to the remote REM measurement sites due to the fact that particles reaching REG and REM were more aged and consequently more internally mixed with other species compared to URB, thus increasing the MAC.

Hereinafter, we will use black carbon (BC) as a common term when comparing the model results (mass of elemental carbon) with the measurements.

2.2.3. *Online chemistry measurements*

Concentrations of the non-refractory components of PM_1 with 30 min time resolution or less were obtained in URB with a quadrupole aerosol chemical speciation monitor (Q-ACSM; Aerodyne Research Inc.). Q-ACSM is an aerosol mass spectrometer (AMS) adequate for long-term deployments in the field. It determines online ambient mass concentrations of submicron SO_4^{2-}, NO_3^-, Cl^-, NH_4^+, and OA. The measurement of OA allows for the characterization of the oxidation state of the organic fraction. The instrument also generates organic mass spectra, which can be further analyzed using multivariate mathematical techniques like positive matrix factorization (PMF). This analysis can help identify the origin or types of OA present in the sample. OA sources for URB for the year 2018 were recently presented in Via et al. (2021). The OA sources were: HOA (hydrocarbon-like organic aerosol a surrogate of primary combustion OA indicative for example of traffic emissions), COA (cooking organic aerosols), BBOA (in this case primary biomass burning organic aerosols) and different OOA types (oxygenated organic aerosols). The OOA component were further deconvolved into two OOA subtypes that differ in volatility and degree of oxidation: less oxidized OOA (LO-OOA) and more-oxidized OOA (MO-OOA). Less or more oxygenated OA relates to less or more aging of OA. The sources found in URB are typically observed in Europe through AMS techniques (Jimenez et al., 2009; Ng et al., 2010; Chen et al., 2022). It should be noted that the uncertainties for the modelled OA factors (due to rotational uncertainty and statistical variability in the sources) can reach up to ± 40% for specific secondary organic aerosols sources (Chen et al., 2021).

2.2.4. Offline chemistry measurements

Q-ACSM measurements were not available for REG and REM stations during the period studied here, the year 2018. Consequently, the mass concentrations of OC at the three sites were determined from 24 h sampled $PM_{2.5}$ filters using a thermal-optical carbon analyzer (SUNSET), using protocol EUSAAR_2 (Cavalli et al., 2010).

To compare model outputs (organic aerosol mass) and observations, an organic-mass-to-organic–carbon (OM:OC) ratio of 1.7 is assumed in URB, this ratio was chosen based on the work of Minguillón et al. (2011), which suggests a greater influence of primary organic aerosols, such as those from vehicle emissions, thus leading to a lower OM:OC ratio. On the other hand, at REG and REM, a higher ratio of 2.1 was adopted, aligning with Karanasiou et al. (2020). The higher ratio at these sites reflects a larger contribution from secondary organic aerosols, which typically possess a higher OM:OC ratio due to processes like the atmospheric photo-chemical oxidation of volatile organic compounds.

2.2.5. Source contribution derived from Aethalometer measurements

The determination of fossil and non-fossil relative contributions to the measured concentrations of BC particles in URB, REG and REM were obtained applying the Sandradewi model (Sandradewi et al., 2008) to the absorption measurements performed with AE33 aethalometers (Magee Scientific; Drinovec et al., 2015) available in the three sites.

Briefly, the AE33 measures the attenuation of light by aerosol particles collected onto a fiber filter tape at 7 different wavelengths (370, 470, 520, 590, 660, 880, and 950 nm). The absorption properties of collected particles were then calculated from the attenuation measurements at the seven wavelengths following the procedure described in Yus-Díez et al. (2021).

The Sandradewi model is based on the fact that non-fossil sources of BC also emit OA with absorption properties (BrC) that strongly enhance the absorption of light in the ultraviolet wavelength range compared to that in the near-infrared range, where BC dominates the absorption. Light absorption Multi-wavelength Aethalometer measurements can therefore be used to quantitatively assess the source contribution of non-fossil (e.g. wood burning) versus fossil sources (e.g. traffic, shipping, industry, etc) to BC concentrations as it was shown in Sandradewi et al. (2008). It is important to note that the BC source apportionment from the Sandradewi model has a rather high uncertainty (not less than 20%) due to specific assumptions in the model (e.g., chosen Absorption Angstrom Exponents or equal Mass Absoprtion Cross section of BC emitted from fossil and non-fossil sources).

2.3. Model description

2.3.1. The MONARCH atmospheric chemistry model

The MONARCH model (Jorba et al., 2012; Badia and Jorba, 2015; Badia et al., 2017; Klose et al., 2021) consists of advanced chemistry and aerosol packages coupled online with the Nonhydrostatic Multiscale Model on the B-grid (NMMB; Janjic et al., 2001; Janjic and Gall, 2012). The model allows running both global and regional simulations with telescoping nests. Multiple choices of gas- and aerosol chemistry schemes can be selected in the model, here we describe the configuration used in this work.

The gas-phase chemistry solves the Carbon Bond 2005 chemical mechanism (CB05; Yarwood et al., 2005) extended with chlorine chemistry (Sarwar et al., 2012). The CB05 is well formulated for urban to remote tropospheric conditions, and it uses photolysis rates computed with the Fast-J scheme (Wild et al., 2000) considering the physics of each model layer (e.g., clouds, absorbers such as ozone). A mass-based aerosol module describes the life cycle of dust, sea salt, BC, OA (both primary and secondary), sulfate, ammonium and nitrate aerosol components (Spada, 2015). A sectional approach is used for dust and sea salt, while the other aerosol species are represented by a fine mode except nitrate which is extended with a coarse mode to consider the condensation of nitric acid on coarse particles (see Table S1 for the microphysical properties of each component). Sulfate production considers the gas-phase oxidation of both sulfur dioxide (SO_2) and dimethyl sulfide, and the aqueous chemistry of SO_2. The heterogeneous hydrolysis of N_2O_5 contributes to the production of nitric acid following the parameterization of Riemer et al. (2003). A thermodynamic equilibrium model (Metzger et al., 2002) solves the partitioning of semivolatile inorganic aerosol components in the fine mode, and an irreversible uptake reaction accounts for the production of coarse nitrate on dust and sea salt (Hanisch and Crowley, 2001; Tolocka et al., 2004). Different meteorology-driven emissions are computed online in MONARCH (i.e., mineral dust, sea salt, and biogenic gas species). The mineral dust scheme of the model is described in detail in Pérez et al. (2011) and Klose et al. (2021). Sea salt emissions are calculated following the source function of Jaeglé et al. (2011) as described in Spada et al. (2013), while the biogenic NMVOC and soil NO emissions are estimated with the Model of Emissions of Gases and Aerosols from Nature (MEGAN) v2.04 model (Guenther et al., 2006).

Black carbon is represented in MONARCH following Chin et al., 2002. Two primary hydrophobic/hydrophilic modes are defined with an ageing process converting mass from the hydrophobic to the hydrophilic mode with a lifetime of 1.2 days. Primary emissions are assumed to be emitted as 80% hydrophobic.

The "simple scheme" proposed in Pai et al. (2020) is adopted to model OA. It is computationally efficient and reproduces well the organic mass assuming fixed SOA yields adjusted to match results from more complex volatility based scheme approach. Despite the substantial differences between the design of "simple" and "complex" schemes, both perform comparably in their ability to capture the observed variability, with coefficients of determination of 0.41 and 0.44, respectively (Pai et al., 2020). Furthermore, the "simple scheme" allows a clear tagging method more difficult to implement with other approaches. Here, we detail briefly the scheme. Primary emissions are emitted as 50% hydrophobic species with an OM:OC ratio of 1.4, while the hydrophilic oxigenated component assumes an OM:OC ratio of 2.1. Similarly to BC, an atmospheric aging of hydrophobic to hydrophilic primary species is simulated with a conversion lifetime of 1.15 days. No marine primary organic aerosol is considered in our implementation. The scheme includes sources of SOA precursors from biogenic, pyrogenic and anthropogenic origin with fixed SOA yields. Biogenic sources of SOA uses a 3% yield for isoprene and 10% yield for both monoterpenes and sesquiterpenes. A 50% of biogenic SOA is emitted directly to account for the near-field formation of SOA. On the other hand, precursors from combustion emissions are scaled from CO emissions as a proxy, of which 1.3% come from fires and biofuels (combustion sources) and 6.9% from fossil fuels. The gas-phase SOA products converts to the aerosol phase based on a first-order rate constant with a lifetime of 1 day.

2.3.2. The HERMESv3 emission model

The High-Elective Resolution Modelling Emission System version 3 (HERMESv3; Guevara et al., 2019; Guevara et al., 2020) is used to provide anthropogenic, biomass burning, and ocean emissions to be used as input in the MONARCH model. HERMESv3 includes two main components: (i) a global-regional module (HERMESv3_GR; Guevara et al., 2019) where the user can flexibly define combinations of existing up-to-date gridded global and regional emission inventories and apply country-specific scaling factors and masks; and (ii) a bottom-up module (HERMESv3_BU; Guevara et al., 2020) that allow computing emissions for Spain at the source level (e.g., road link) combining state-of-the-art bottom-up methods with local activity information and emission factors. Detailed databases for Spain are used within the HERMESv3_BU to produce a refined emission inventory for the country.

2.4. Emission inventories

In this study, we aim to evaluate the main uncertainties associated with the description of CAs in NE Spain by comparing results obtained

from three different anthropogenic emission inventories in Spain (Table 2). Specifically, we utilize two versions of the European-scale emission inventory CAMS-REG_v4 (Kuenen et al., 2022), developed under the Copernicus Atmosphere Monitoring Service (CAMS), as well as a detailed national inventory for Spain that is computed using HERMESv3_BU. For ease of reference throughout the rest of the text, we will label these emission inventories as CRV42, CRV42_REF2, and Hv3_BU.

The CRV42 inventory provides gridded emissions for Europe for the main atmospheric pollutants and greenhouse gases: NO_x, SO_2, non-methane volatile organic compounds (NMVOCs), NH_3, CO, PM_{10} and $PM_{2.5}$, and CO_2 and CH_4 (Kuenen et al., 2022). CRV42 has been built using the official emission data reported by each European country for each source category to the United Nation Convention on Climate Change, the Convention on Long-Range Transboundary Air Pollution and the European Union National Emission Ceilings Directive. Its main advantage is that it considers country-specific information on technologies, practices, and associated emissions. Emissions are given for different sectors using the Gridded Nomenclature For Reporting (GNFR) sectorization. The raw emission inventory maintains a consistent spatial resolution of $0.1^\circ \times 0.05^\circ$(approximately 11 x 6 km) throughout Europe; it was released in 2020 providing emissions for an 18-year time series (2000–2017) consistently. The CRV42 inventory reports total annual emissions, and hourly emissions can be derived through the application of temporal profiles (i.e., monthly, weekly and diurnal) per GNFR sector based on Kuenen et al. (2003) or of more detailed temporal profiles recently proposed by Guevara et al. (2021); here we use the former. Additionally, speciation profiles for PM (EC, OC (expressed in full molecular mass), sulfate, sodium and other minerals) and NMVOCs (split into 25 hydrocarbon groups as classified by the Global Emissions InitiAtive (GEIA)) are provided per GNFR sector, country and year.

As a complementary dataset, the CRV42_REF2 is a science version of CRV42 using a consistent approach for RWC PM emissions. Denier Van Der Gon et al. (2015) identified inconsistencies in how wood combustion emissions were reported in European inventories mainly due to inconsistencies in emission factors used by countries. A relevant aspect of this inventory (v4.2_ref2) is that PM emissions ($PM_{2.5}$ and PM_{10}) from GNFR_C (other stationary combustion) were replaced with a bottom-up estimate (Denier Van Der Gon et al., 2015; Kuenen et al., 2022). This bottom-up approach considers activity data (wood usage and appliance types), consistent emission factors across Europe for RWC, including condensable fraction, for both wood and solid fuels, and spatial distribution based on population density and own wood consumption map. Besides GNFR_C sector, CRV42_REF2 incorporates the other sectors as present in CRV42. CRV42_REF2 tries to overcome the inconsistencies between countries and limitations in modeling works such as source attribution (Simpson et al., 2020).

The third inventory used in this study is the Spanish emission inventory computed using the HERMESv3_BU emission model. Hv3_BU is designed to provide bottom-up emissions from point sources (energy and manufacturing industries), road transport, residential and commercial combustion, other mobile sources, and agricultural activities (livestock and use of fertilizers). A comprehensive compilation of activity data from multiple sources of information is combined along with emission factors based on EMEP and EEA (2019) and meteorology information to derive final gridded emission estimates at hourly resolution. For the residential sector, Hv3_BU considers the following types of fuels: natural gas, liquefied petroleum gas (LPG), heating diesel oil, wood, and coal. Note that this inventory already considers the condensable fraction of RWC PM, as reported in the EMEP/EEA emission inventory guidelines.

Regarding the RWC emissions, the three datasets considers the inclusion of condensable fraction in Spain, although CRV42 drags the inconsistency among different countries. One of the major differences between them is how RWC PM emissions are speciated (Table 2). The addition of condensable fraction implies an increase of OC mass emitted while EC should not be affected. Therefore, the speciation of EC/OC changes significantly from a 48.6/40.6% of the total $PM_{2.5}$ in CRV42 (which neglects condensables in the speciation) to 9.8/87.7 and 7/75% in CRV42_REF2 and Hv3_BU, respectively. Remarkably, this results in an unexpected decrease in EC emissions for CRV42_REF2 in contrast to CRV42 in Spain, essentially rectifying the inconsistency inherent in CRV42.

Another relevant difference among the inventories is the spatial allocation of RWC as will be discussed in Section 3.1.

For areas outside of Spain, as well as for shipping and biomass burning emissions, the same emission datasets are consistently used: CAMS-REG_v4 and GFAS (Global Fire Assimilation System). These datasets are processed using the HERMESv3_GR module, which ensures a standardized and efficient approach in handling emissions data for modeling purposes.

Table 2
Main characteristics of the three emission inventories used in this study.

	CRV42	CRV42_REF2	Hv3_BU
Air pollutants	NOx, SO_2, NMVOC,NH_3, CO,PM_{10},$PM_{2.5}$	NOx, SO_2, NMVOC,NH_3, CO,PM_{10},$PM_{2.5}$	NOx, SO_2, NMVOC,NH_3, CO,PM_{10},$PM_{2.5}$
Reference year	2017	2017	2018
Domain	Europe	Europe	Spain
Spatial resolution	0.1x0.05 deg	0.1x0.05 deg	User configurable (5–1 km)
Temporal resolution	Yearly	Yearly	Hourly
condensable fraction RWC	Not consistently	Yes	Yes
EC fraction RWC[a]	0.4866	0.0989	0.07
OC fraction RWC[a]	0.4068	0.8778	0.75[b]
Reference	Kuenen et al., 2022	Denier Van Der Gon et al., 2015; Kuenen et al., 2022	Guevara et al., 2020

[a] RWC EC/OC speciation for Spain as reported by Kuenen et al., 2022
[b] Emissions compute organic mass and assumes OM:OC of 1.8 for RWC and 1.4 for other sources, as suggested by Klimont et al., 2017

2.5. Model setup

We configured the MONARCH model using different setups to conduct the simulations of this work (Table 3). Three nested domains were designed to cover the European continent and part of North Africa with a horizontal resolution of ~ 20 km (D01), Spain at a resolution of ~ 5 km (D02), and NE Spain at a resolution of ~ 1 km (D03) as shown in Fig. 1. Model runs used one, two or the three nested domains and a combination of the emission inventories described in Section 2.4. The brute force method was used to apportion the contribution of residential emissions (CAMS: GNFR_C; Hv3_BU: residential and commercial combustion), traffic emissions (CAMS: GNFR_F1-F2-F3-F4; Hv3_BU: road transport), shipping emissions (CAMS: GFNR_G; Hv3_BU: shipping), and biomass burning emissions (GFAS) on BC/OA concentrations. Only a two-domain configuration was used for the source apportionment (SA) run.

The model ran with 24 vertical layers and a top of the atmosphere set at 50 hPa. Meteorology initial and boundary conditions were obtained from the ECMWF global model forecasts at 0.125°and chemical boundary conditions from the CAMS global model forecasts at 0.4° (Flemming et al., 2015). The HERMESv3 system was used to process the anthropogenic emissions described in Section 2.4, the biomass burning emissions (forest, grassland, and agricultural waste fires) from the GFASv1.2 analysis (Kaiser et al., 2012), and ocean DMS emissions from CAMS_GLOB-OCEANv1.1 (Lana et al., 2011; Granier et al., 2019). HERMESv3 remapped the original datasets into the model domains and

Table 3
Simulations performed.

Run	Description	Domain	Emiss. Inv.	Sector tagged
1	Simulation based on the European-scale emission inventory.	D01-D02	CRV42	None
2	Simulation based on science version of the European-scale emission inventory.	D01-D02	CRV42_REF2	None
3	Simulation based on local HERMESv3 emission inventory.	D01-D02	CRV42_REF2 (Europe except Spain)/Hv3_BU (Spain)	None
4	Simulation using three domains, with the science version of the European-scale emission inventory applied to the first domain, and the HERMESv3 inventory used for domains D02 and D03.	D01-D02-D03	CRV42_REF2 (D01)/Hv3_BU (D02-D03)	None
5	Simulation based on the science version of the European-scale emission inventory for Domain D01 and the local HERMESv3 emission inventory for Domain D02, with specific sectors tagged.	D01-D02	CRV42_REF2 (D01)/Hv3_BU (D02)	GNFR_C/ residential GNFR_F/ road transport GNFR_G/ shipping GFAS

derived hourly and speciated emissions.

Annual emission of CAMS inventories were speciated and broken down into hourly resolution as described in Section 2.4. Emissions from CAMS were used for Europe while Hv3_BU was used for Spain in specific model runs. The autosubmit workflow manager was used for efficient execution of the MONARCH modeling chain (Manubens-Gil et al., 2016).

2.6. Evaluation metrics

We evaluate the model performance using quantitative statistical metrics, as outlined in Table S2. These metrics include Normalized Mean Bias (NMB), Normalized Mean Error (NME), Pearson Correlation Coefficient (PCC), Fraction of Predictions within a Factor of Two (FAC2) of observations, Fractional Bias (FB), bias, and Root Mean Square Error (RMSE).

Emery et al. (2017) suggest benchmarks for assessing the performance of photochemical models, particularly for species such as EC and OC. They base their recommendations on the "goal" and "criteria" targets proposed by Boylan and Russell (2006). The "goal" represents the optimal performance a model can be expected to achieve, while the "criteria" refers to an "acceptable model", which should be considered as a performance level that a majority of models can attain.

Table S2 presents the benchmarks proposed by Emery et al. (2017) for NME and NMB. Although they suggest using three metrics to evaluate the model, they do not provide benchmarks for PCC due to substantial statistical uncertainty in determining the 33rd and 67th percentiles. Additionally, other recommended values for FB for PM (Boylan and Russell, 2006) and FAC2 (Chang and Hanna, 2004; Soni et al., 2021) are included.

3. Results

3.1. Spatio-temporal variability of anthropogenic emissions in Spain

In this section we analyze the main differences between the three emission inventories used (CRV42, CRV42_REF2 and Hv3_BU) in terms of spatial and temporal distribution. The annual emissions of $PM_{2.5}$ from RWC for Spain estimated by CRV42, CRV42_REF2 and Hv3_BU are 54.4, 68.8 and 63.9 kt, respectively. Fig. 2 depicts the spatial distribution of RWC emissions of CRV42_REF2 and Hv3_BU over a gridded domain at 5 km horizontal resolution. While the CRV42_REF2 inventory shows a distribution of RWC towards urban areas, the Hv3_BU methodology assigns them more in rural regions. In both CRV42 and CRV42_REF2, RWC emissions are spatially distributed using a specific European proxy that takes into account population density, degree of urbanisation and also proximity to wood (Kuenen et al., 2022). The resulting spatial pattern principally follows population distribution but is also influenced by local wood availability. On the other hand, Hv3_BU combines the fuel statistic consumption of the residential sector at NUTS level 3 with the Global Human Settlement Layer (GHSL) population density and settlement category (urban, rural) data (Florczyk et al., 2019) to spatially allocate residential emissions. For natural gas, emissions are allocated in urban areas while for wood in rural ones (Guevara et al., 2020). The use of biomass fuel for residential heating is not a common practice in cities across Spain and the total population density as a proxy to distribute RWC in the country may introduce a significant bias in modeling results as will be shown in the following sections. Kuenen et al. (2022) already identified this as a possible limitation in the CAMS European inventories. However, this assumption may still be appropriate for other countries such as Norway (López-Aparicio et al., 2017) or Greece (Grythe et al., 2019; Athanasopoulou et al., 2017).

When looking at the temporal distribution of EC, OC and $PM_{2.5}$ emissions estimated by each of the three datasets, relevant methodological differences arise in the temporal disaggregation, the attribution to specific sectors, and the EC/OC speciation assumed. Fig. 3 shows the monthly distribution of total anthropogenic emissions for $PM_{2.5}$ (a, b), EC (c, d), and OC (e, f) for each emission inventories used over Spain (left panels) and over Barcelona city (right panels). The emissions are split into *residential*, on-road *traffic*, and *others* sectors. In both CRV42 and CRV42_REF2, *residential* contribution comes from the other stationary combustion (GNFR_C sector), *traffic* contribution includes road transport exhaust gasoline/diesel/LPGgas (GNFR_F1-F2-F3 sectors) and road transport non-exhaust (GNFR_F4 sector, which includes wear emissions from brakes, tires and the road), and the *others* contribution represents all the other emission sectors included in the inventory, mainly public power (GNFR_A sector), industry (GNFR_B sector), fugitives (GNFR_D sector), solvents (GNFR_E sector), shipping (GNFR_G sector), aviation (GNFR_H sector), offroad (GNFR_I sector), waste (GNFR_J sector), agriculture livestock (GNFR_K sector), and agriculture others (GNFR_L sector). For Hv3_BU, the residential emissions include emissions of residential and commercial combustion from natural gas, LPG, heating diesel oil, wood and coal combustion processes; traffic contribution is represented by road transport categorized as in COPERTv5 for vehicle categories for both exhaust (hot and cold start) and non-exhaust (wear and resuspension); *others* contribution includes point sources sector (energy and manufacturing facilities and waste incinerators), shipping in ports, aviation, recreational boats, livestock, agricultural crop operations, agricultural machinery, and agricultural fertilizers. For the *residential* and *traffic* categories, all three inventories consider the same emissions sources except for road transport resuspension, which is only estimated by Hv3_BU using emission factors from a measurement campaign performed in Barcelona (Amato et al., 2012). Nevertheless, while resuspension is an important contributor to total primary PM_{10}, its contribution to $PM_{2.5}$ and primary CAs emissions is very limited (Rodriguez-Rey et al., 2021). The CAMS inventories follow a V-shape seasonality, dominated by the residential sector, in $PM_{2.5}$, EC

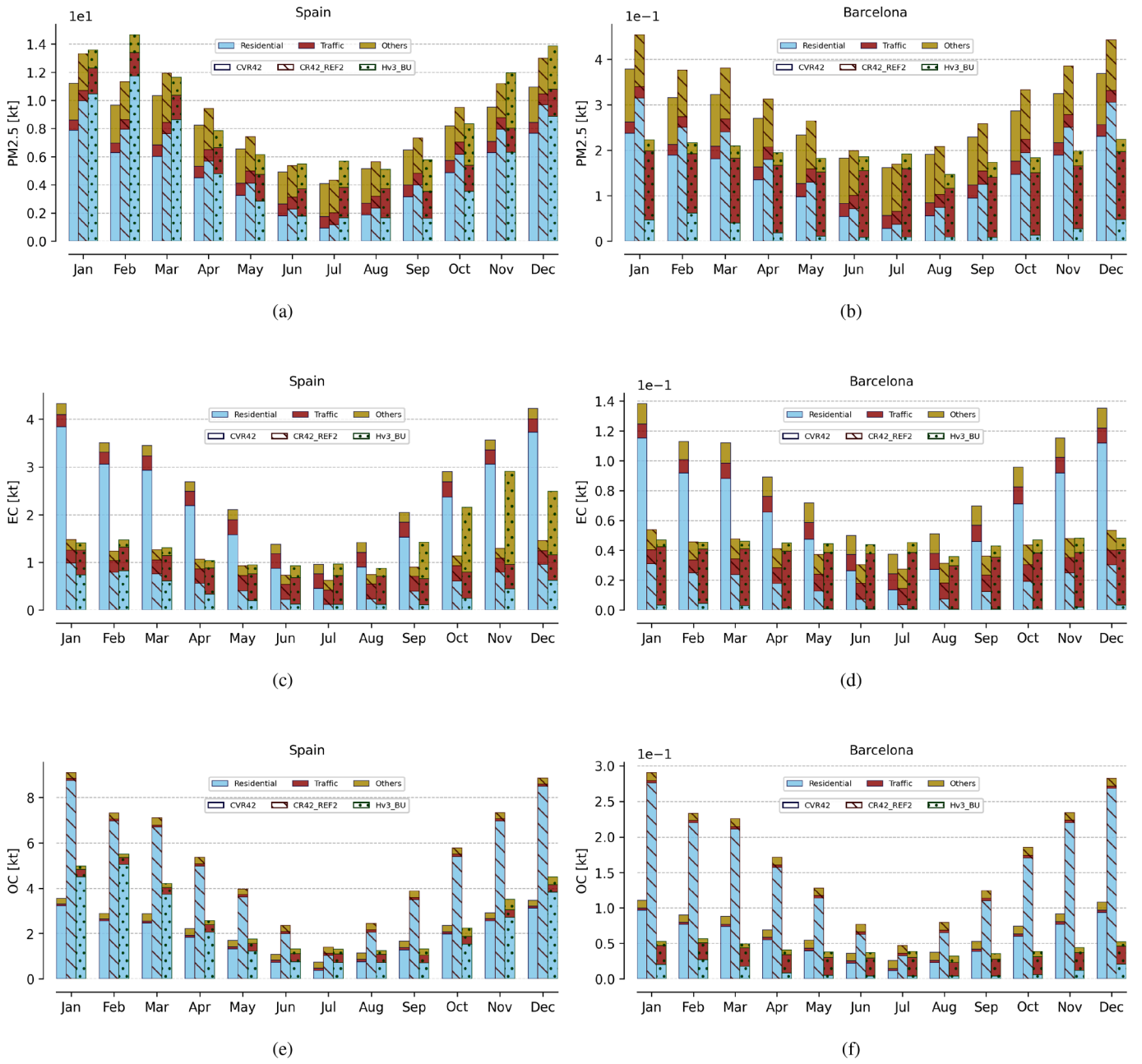

Fig. 3. Monthly anthropogenic emissions of (a,b) fine particulate matter ($PM_{2.5}$), (c,d) elemental carbon (EC), and (e,f) organic carbon (OC) derived from CRV42, CRV42_REF2 and Hv3_BU inventories over Spain (a,c,e) and the city of Barcelona (b,d,f). Emissions are split in *residential* sector (light-blue), on-road *traffic* emissions (red), and the remaining as *others* emissions (dark-gold). An area of 30 km × 30 km centered in URB station is used to compute the Barcelona emissions. Note that Hv3_BU only includes shipping emissions in ports within *others*.

and OC. Specifically, *residential* emissions peak during wintertime while *traffic* and *others* are rather constant throughout the year. For $PM_{2.5}$, a slight increase is detected during March and April in *others* emissions, mainly attributed to agriculture activity. On the other hand, Hv3_BU uses specific profiles per sector with relevant differences compared with the previous ones. A combination of monthly and weekly time factors are used for all sectors except for residential and livestock/agricultural fertilizers emissions, where a day-of-year time distribution based on the heating degree-day approach (Guevara et al., 2021) and the Skjøth et al., 2011 meteo-dependent parameterizations are used, respectively. In the case of road transport emissions, the seasonality of Hv3_BU emissions is derived from observed traffic count datasets. This results in *residential* emissions peaking in February, which is likely related to the cold spell felt throughout Europe during February 2018 (Copernicus, 2018), *traffic* emissions showing a clear reduction during August in Barcelona, when people are away for holidays, and *others* emissions showing a relevant increase during October-November-December mainly due to the activity attributed to agricultural machinery.

Major differences are found in the distribution of total emissions per sector. The case of the Barcelona city is a good example of how the inventories describes the contribution of the total $PM_{2.5}$ emissions to different sectors. While Hv3_BU suggests that traffic is the dominant source of $PM_{2.5}$ emissions in the city of Barcelona, both CRV42 and CRV42_REF2 assign a larger share of these emissions to the residential sector.

Specifically, on an annual basis, CRV42 assigns 50.2% to the residential sector and 10.2% to traffic, while CRV42_REF2 assigns 57.5% to the residential sector and 8.8% to traffic. The difference in allocation

may stem from the level of detail and specificity in the information used by each inventory, with Hv3_BU providing more granular insights on Spain and Barcelona. In contrast, Hv3_BU accounts for 12.9% of $PM_{2.5}$ emissions in the residential sector and 72% in traffic for Barcelona in 2018.

Finally, the treatment of condensable fraction in the *residential* sector introduces another source of relevant differences between CRV42 and the other two inventories. While the *residential* $PM_{2.5}$ emissions are rather consistent in both CAMS inventories, the speciation used to derive EC/OC emissions (see Table 2) reduces EC emissions around a factor 4 in the CRV42_REF2 compared with CRV42 and increases OC emissions above factor 2. This discrepancies is due to the fact that in CRV42 the speciation proposed for RWC assumes that condensable compounds are not included in the national emissions used as input in the CAMS inventory. Nevertheless, in the case of Spain the condensable fraction is actually considered in official reported emissions (Fagerli et al., 2019) and subsequently in the CRV42 inventory. In Spain, the EC emissions estimated by Hv3_BU are generally consistent with CRV42_REF2. It is important to note, however, the significant increase observed in EC emissions during autumn months (September-December) at a national scale in Hv3_BU. These increased emissions, predominantly linked to the *others* sector, are driven by the activity of agricultural machinery. Interestingly, this escalation in emissions during the autumn season is not reflected in the observational data that will be analyzed in the following sections, underscoring the need for regionally-specific refinements when developing emission inventories.

All in all, relevant uncertainties are still present in the methodologies and datasets used to derive emission estimates for a specific country or region. In the following sections we evaluate the MONARCH model with detailed measurements to provide further insights in the differences identified between inventories.

3.2. Differences in CA concentrations obtained with the three emission inventories

The way in which the fraction of condensable material is included in RWC emissions strongly impacts the results of the chemistry model. Fig. 4 shows the monthly average surface concentration of BC (left column) and OA (right column) at the three EGAR-IDAEA sites (URB, REG, REM) simulated by the model at ~ 5 km horizontal resolution (~ 20 km results shown in Fig. S2) using the three emission inventories described in Section 2.4 (Run-1, Run-2 and Run-3 in Table 3). In all simulations, the condensable fraction is included as primary emissions. Run-2 and Run-3 results capture reasonably well the monthly variability and concentrations of BC in the three sites, meanwhile Run-1 shows a systematic overestimation during wintertime. The treatment of RWC emissions in Run-2 and Run-3 are more consistent with observations. The main differences with Run-1 can be explained by the important change in the speciation profile (see Table 2) more than by a possible change in total $PM_{2.5}$ emissions reported by the inventories for Spain (Fig. 3ac). Note the deviation in REG and REM sites since October in Run-3, which we attribute primarily to the activity of agricultural machinery that has significant impact on EC in the Hv3_BU emission inventory (Fig. 3c). It is important to recognize the uncertainties and potential overestimation associated with the bottom-up approach, particularly for sectors such as agriculture where quantifying activities can be challenging. Future work could benefit from more detailed characterization and quantification of these emissions, possibly complemented by new activity and observational data.

Furthermore, the spatial distribution of BC surface concentration is also rather consistent between Run-2 and Run-3 (Fig. S3). Major differences are found in Run-1 where large areas of the domain show concentrations above 1.0 μ/gm^3 in January, not detected in EGAR-IDAEA sites nor simulated in the other two runs. This findings are supported by both ~ 20 km and ~ 5 km model runs consistently.

Regarding OA, Run-2 overestimates the two other runs and observations in URB and REG sites, contrary to BC results (Fig. 4). The overestimation could be attributed to the increase in OA emissions due to the condensable fraction (new speciation profile), however, Run-3 is still consistent with observations. Considering that both Run-2 and Run-3 use similar approaches in the treatment of RWC, the higher concentrations in Run-2 are attributed to a limitation in the spatial distribution of the emissions (Fig. 2). As noted in Section 2.4, the Hv3_BU model uses other information a part from population to allocate RWC emissions (e.g., settlement information). This approach results with more consistent OA compared with the observations. REM is a remote site located far

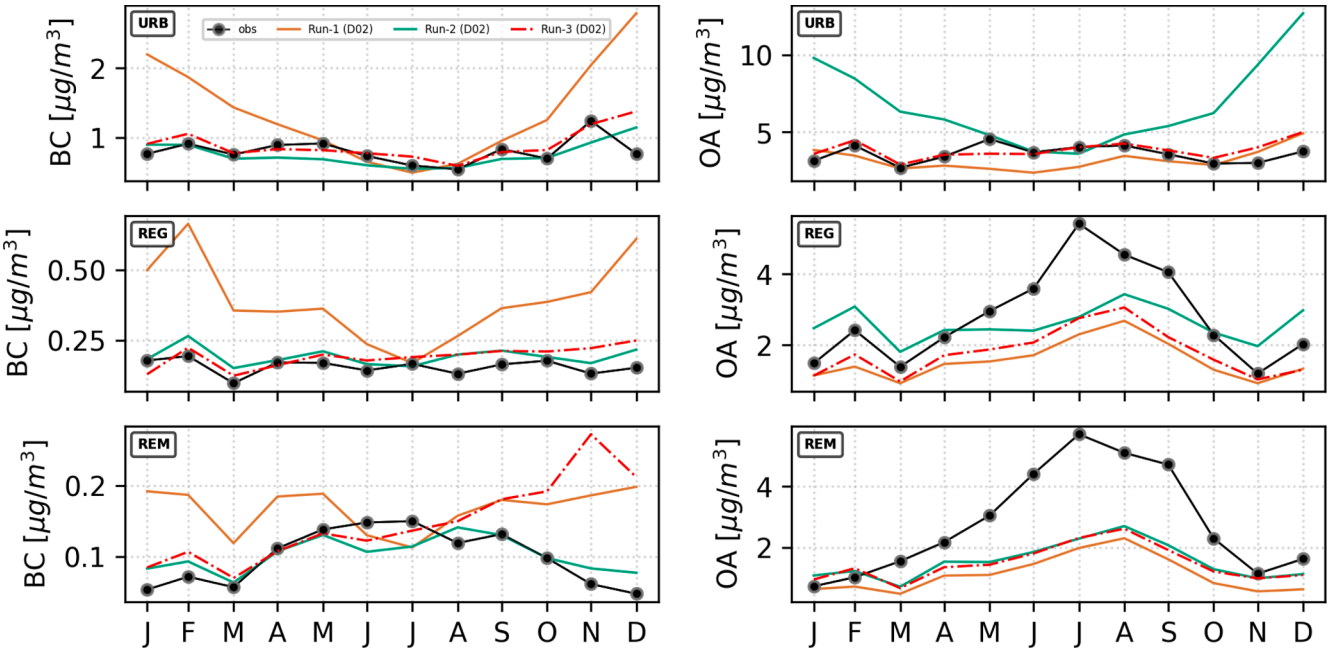

Fig. 4. Monthly mean observed (black line) and modeled surface concentrations of BC (left) and OA (right) at URB, REG, and REM sites using three emission inventories (CRV42 orange line, CRV42_REF2 cyan line, and Hv3_BU dash-dotted red line) for 2018. Results of D02 at ~ 5 km horizontal resolution. OA observations are derived from filters.

from emission sources and not sensitive to the spatial distribution of emissions, while URB and REG, more influenced by urban activities, detect the issue during wintertime. None of the three runs is able to reproduce the increase of OA during summertime, particularly relevant in REG and REM, pointing to a lack of secondary organic aerosol production from biogenic sources in the model.

Finally, it is worth to mention the role of the temporal disaggregation of emissions used in the different inventories. For instance, observations show an increase in BC/OA concentrations from January to February in 2018, a feature captured by Hv3_BU and not by CAMS inventories in URB site mainly due to the specific methodologies used in the different datasets, as discussed in Section 3.1.

From Run-1, Run-2 and Run-3 results, the benefit of implementing condensable fraction in RWC over the area of study is demonstrated. In the following sections, we investigate the contribution of key emission sectors to CA concentrations using only CRV42_REF2 and Hv3_BU inventories.

3.3. Black carbon surface concentration and source contribution

To understand how different emission sectors contribute to CA concentrations and the role of resolution, we have run the model with a nested configuration tagging the contributions from the *residential*, *traffic*, *shipping*, *fires* (biomass burning) and *other* emission sources (see Section 2.5). First, we evaluate and discuss BC results of Run-4 in terms of model resolution compared against observed BC concentrations at the three monitoring sites. On a second stage, we quantify the source attribution based on Run-5 and discuss the main uncertainties derived from the emission inventories used.

Table 4 presents the annual evaluation of Run-4. Statistics are computed over daily averages and presented for complete 2018 year for the three domains (D01: $\sim$ 20 km, D02: $\sim$ 5 km, D03: $\sim$ 1 km) at URB, REG and REM sites. Results met the model performance goal proposed by Emery et al., 2017 for NME throughout all the year in URB, only in summer the criteria is not met for NMB for D01 (see Table S3). Whereas REG metrics are within the recommendations (particularly for D02 and D03), REM site shows systematic overestimations. The concentrations observed in REM are very low ($<0.2\ \mu g/m^3$) often close or below the detection limit of the MAAP ($0.1 \mu g/m^3$) for several days. This result points toward a model limitation reproducing events characterized by PBL developments below the height of REM station. Overall, PCC is >0.5 during most of the seasons at the three sites (lower in REM). Very good FAC2 values are obtained for URB and REG, particularly for D03. The benefit of using high-resolution is clear in very complex terrain areas like REM. MONARCH meteorology has been evaluated in detail elsewhere (e.g., Sicard et al., 2021). Here, Table S5 shows the annual performance indicators for some meteorological parameters available at URB and REG sites.

The time series of BC daily concentrations at the three sites are shown in Fig. 5. The model presents a good agreement with observations at daily resolution, particularly with D03. The urban-background URB site is well described with both CRV42_REF2 (D01) and Hv3_BU (D02 and D03) emissions, reproducing not only the variability but also the magnitude of BC concentrations. Best model correlations are found during Spring months period, with PCCs values of 0.75, 0.68, and 0.81 for D01, D02, and D03 respectively (see Table S3). The Hv3_BU reports higher emissions in URB (see Fig. 3d), which appears to be consistent with the concentrations measured. Some of the peaks, especially during winter time, are better captured increasing the model resolution. Although some limitation capturing the extreme events, the model is capable to simulate BC concentrations. During summertime (June-July-August), a systematic underestimation is detected in URB. The traffic activity of the city is reduced during summer (mainly August) whereas activities related with the tourism increases (i.e., hotelling of passenger ships in the harbour). In 2018, the Port of Barcelona received a total of 4.5 million passengers, almost 9% more than in 2017 (Port de Barcelona, 2018). A clear indicator of the potential significance of the harbour activity in the city and a possible source of uncertainty in the emissions used in this work. Note that Hv3_BU only includes shipping emissions in ports; over the sea, those are derived from the Copernicus inventories.

Fig. 5b shows BC concentrations at REG, an urban-regional environment affected by air masses advected from the metropolitan area of Barcelona city during the sea-breeze circulation (Jorba et al., 2013). Larger discrepancies between domains are observed in this site despite the low concentrations. D01 presents a clear overestimation during most part of the year, except during summer, whereas better agreement and consistency with the observations are observed with D02 and D03 for all seasons. As discussed in Section 3.1, the monthly profiles of CRV42_REF2 inventory distribute annual emissions with a maxima in January and minima in July mainly driven by residential emissions (Fig. 3c), but observations indicate that BC concentrations during wintertime at REG are much lower compared to the other seasons. A better consistency is reached using Hv3_BU emissions in D02 and D03, where the variability is very well captured. Albeit some deviation is detected from October mainly attributed to the temporal distribution of agricultural machinery emissions assumed in Hv3_BU as discussed previously. The wintertime overestimation of D01 can also be attributed to the spatial distribution of residential emissions. Fig. S5 and Fig. S6 show model results of BC surface concentration and source contribution of the residential, traffic and others emission sectors using CRV42_REF2 and

Table 4
Annual performance indicators of black carbon (BC) and organic aerosol (OA) concentrations at URB, REG, and REM sites, for each domain (Run-4). Values that meet the goal benchmark are shown in italics, while those that meet the criteria benchmark are shown in bold. NMB, NME, and FAC2 are expressed in percentage.

				NMB	NME	PCC	FB	FAC2
Black Carbon	2018	URB	D01	**−33.50**	***39.69***	0.59	**−40.25**	**77.12**
			D02	***−4.09***	***32.56***	0.59	***−4.18***	**90.11**
			D03	***−7.57***	***30.59***	0.62	***−7.87***	**91.81**
		REG	D01	82.05	89.94	0.30	**58.18**	**53.80**
			D02	***15.35***	***40.44***	0.49	***14.26***	**81.87**
			D03	***−7.30***	***34.24***	0.59	***−7.58***	**84.80**
		REM	D01	42.45	**69.60**	0.50	**35.02**	**55.15**
			D02	89.78	109.33	0.11	61.96	48.53
			D03	**20.11**	**53.39**	0.60	***18.27***	**62.87**
Organic Aerosol	2018	URB	D01	**47.08**	**62.11**	0.35	**38.11**	**75.53**
			D02	***5.66***	***27.32***	0.59	***5.51***	**92.55**
			D03	***1.12***	***21.78***	0.75	***1.11***	**97.87**
		REG	D01	**44.87**	70.10	0.25	**36.65**	**60.47**
			D02	**−36.38**	***40.38***	0.82	**−44.47**	**76.74**
			D03	**−43.12**	***44.58***	0.83	**−54.97**	**63.95**
		REM	D01	**−43.48**	**50.28**	0.68	**−55.55**	**59.70**
			D02	**−49.77**	**53.36**	0.71	−66.26	**52.24**
			D03	−60.72	**60.97**	0.81	−87.19	31.34

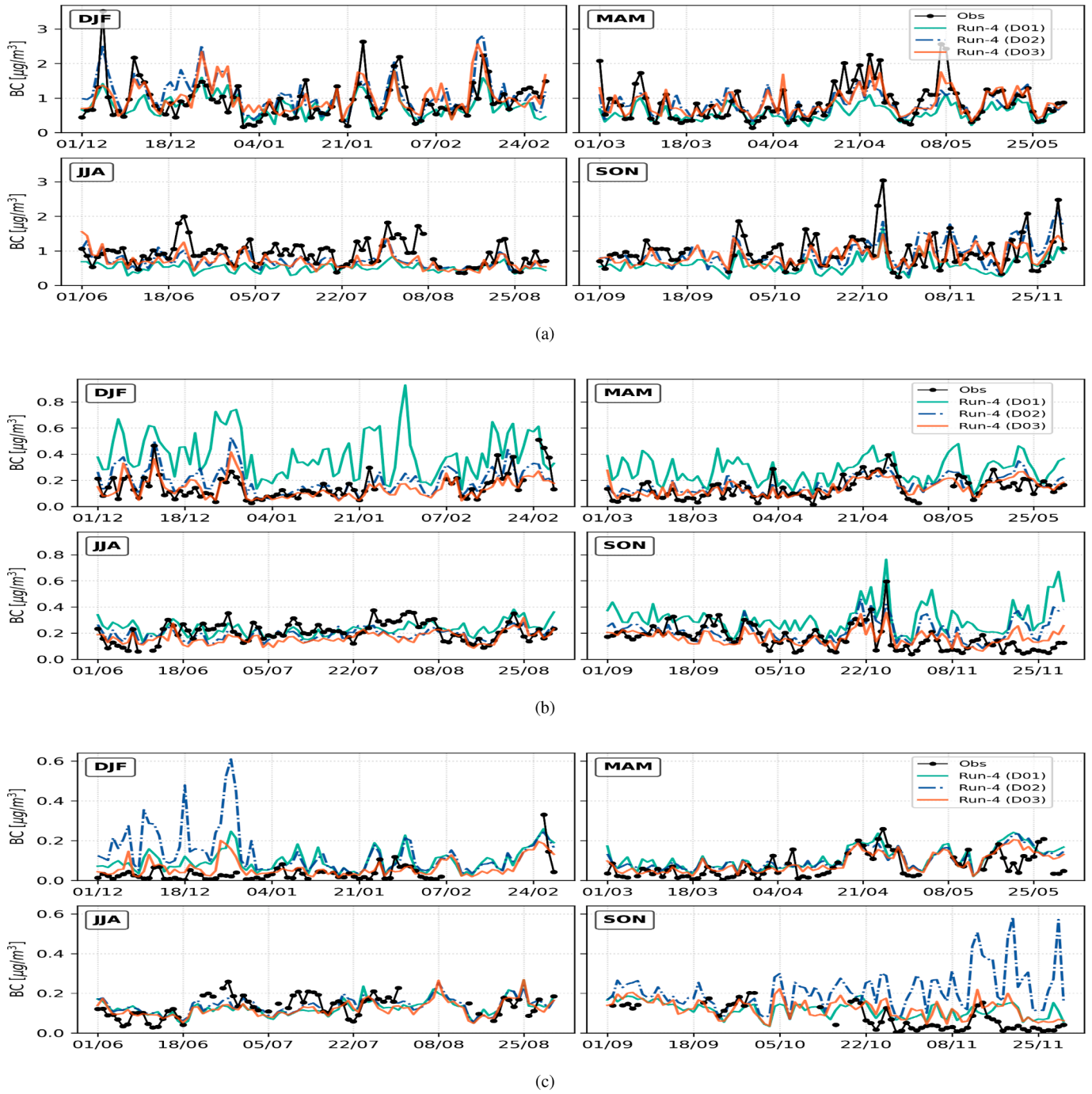

Fig. 5. Time series of daily-average BC concentrations at (a) URB, (b) REG, and (c) REM sites for 2018 (observations black line, Run-4 D01 green line, D02 dashed-dotted blue line, and D03 orange line). Panels grouped in December-January-February (DJF), March-April-May (MAM), June-July-August (JJA), and September-October-November (SON).

Hv3_BU respectively for January and July. One of the major differences of the results is the contribution of residential emissions to BC surface concentrations during January and their spatial distribution. While CRV42_REF2 residential emissions explain a large fraction of REG BC concentrations, this is much lower in the case of using Hv3_BU. Considering the information derived from REG observations, we can conclude that there exist limitations in the methods employed in CRV42_REF2 to distribute the residential emissions (see Section 2.4 and Fig. 2). Finally, the underestimation identified during summer in URB is also observed here, highlighting the close influence of URB air masses on REG site. Overall, both D02 and D03 show clear skills in reproducing BC concentrations measured at REG, even capturing the different peaks observed throughout the year.

Fig. 5c presents BC concentrations at REM, a remote environment with very weak anthropogenic influence. As a remote site located in a high-altitude steep mountain at 1570 ma.s.l., REM is above the planetary boundary layer (PBL) during several periods of the cold season (Pandolfi et al., 2014). Thus, concentrations are very low and sometimes below the detection limit as noted before (signal to noise is low in REM). Observed concentrations reach an annual average of 0.079 $\mu g/m^3$, being much lower than the levels registered in URB (0.93 $\mu g/m^3$) and REG (0.17 $\mu g/m^3$). Such a complex site is challenging to reproduce by the model. Overall, results tend to overestimate the low concentrations

observed at REM, although levels already remain $< 0.2\ \mu g/m^3$. The three domains show very similar results throughout the year except D02 in winter. On one side, results suggest that the model has limitations to reproduce the atmospheric conditions (i.e., stability, thermal inversion) during wintertime. Only the ~1 km resolution can reproduce the very low concentrations for some specific winter periods, but not all of them. On the other hand, D02 overestimates concentrations from September attributed to a combination of the model resolution, atmospheric dispersion, and the temporal profile of the agricultural machinery activity assumed in Hv3_BU. During summertime and spring, the agreement with observations is better and the three domains are consistent among them. As shown in Pandolfi et al. (2014), REM station is within the polluted PBL in summer and spring most of the time. Therefore, one can expect a better representation from the model during this period than wintertime.

To deepen our understanding of the contributions of different emission sectors and their representation in the model, we performed a comprehensive source contribution analysis that integrated both model results and observations. Specifically, we categorized emissions from various sectors, including *residential*, *traffic*, *shipping*, *fires* (GFAS emissions), and *others* (all the remaining emissions), and quantify their contribution based on the model results (Run-5, D01 and D02). Additionally, we applied the source apportionment method detailed in Section 2.2.5 to derive the proportions of fossil and non-fossil emissions from the observations. Through this analysis, we gained a more comprehensive understanding of the relevance of *residential* emissions and their representation in the model, as well as a basis for comparing our model results with observations. Figs. 6 and 7 provide a synthesis of the monthly mean contribution (absolute values and percentage) of black carbon (BC) emission sources to surface concentrations derived from observations and model results, for January and July respectively, at URB, REG, and REM sites.

The first column of the figures presents the contribution of fossil and non-fossil contribution as derived from observations. The second column presents the contribution of different sectors, such as *traffic*, *residential*, *fires*, *shipping*, and *others*, using the CRV42_REF2 emission inventory for the first domain D01 at the three sites. Finally, the third column presents the corresponding results using Hv3_BU emissions for domain D02.

Figs. 6a and 7a show the source contribution derived from observations with *fossil* representing the contribution to the measured BC concentrations from fossil fuel combustion sources (mainly dominated by traffic, and to a lesser extent by other sources like *shipping*, industries and power generation; natural gas, widely used in URB, can be also considered a fossil source of BC), and *non-fossil* describing other than fossil BC sources from combustion of non-fossil fuel like biomass burning

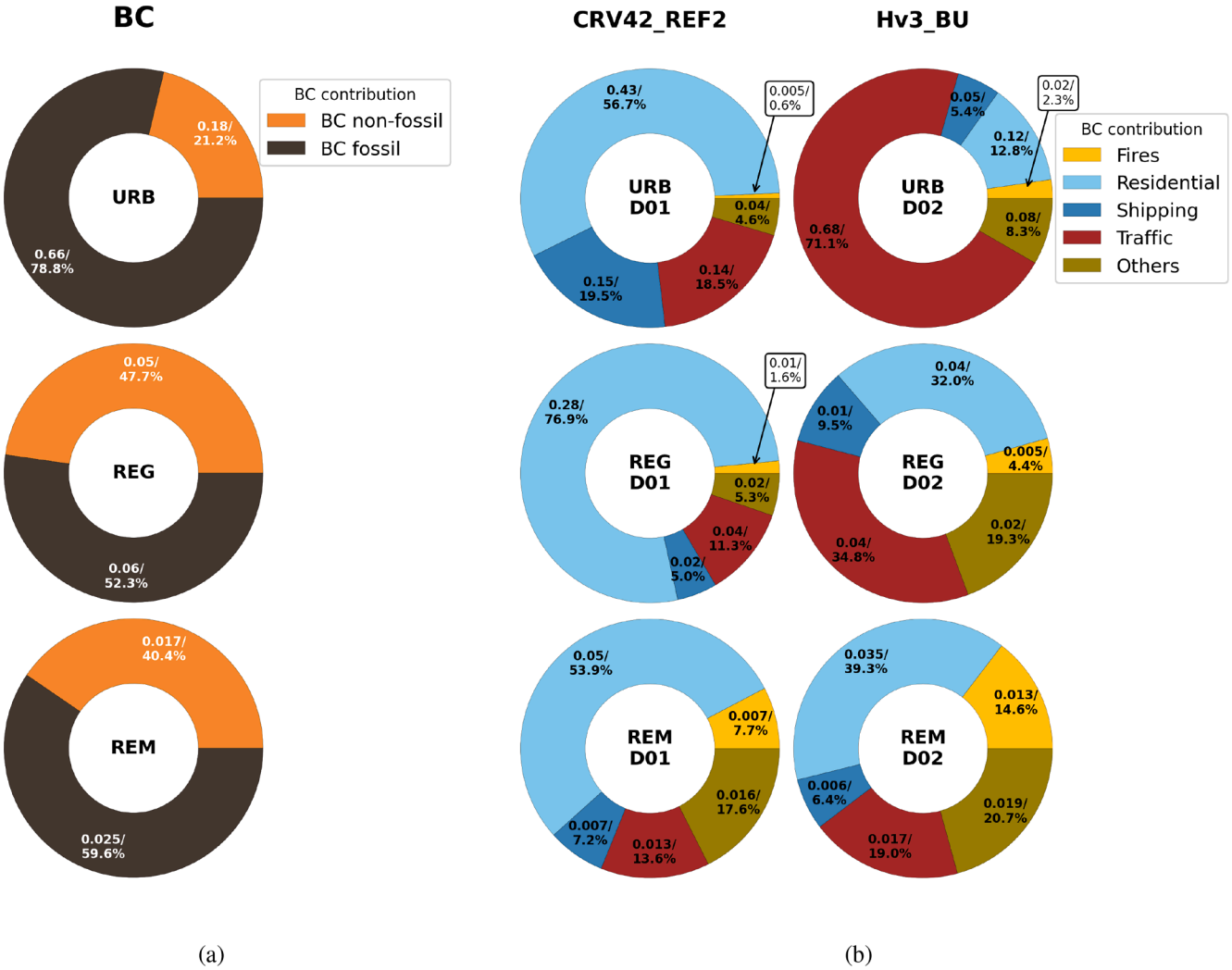

Fig. 6. The monthly mean contribution of BC surface concentration from emission sources for January 2018 at URB, REG, and REM (rows) derived from (a) observations and (b) the MONARCH Run-5 simulation. The columns represent the model results for D01 and D02, and the colors indicate the different emission sources tagged. The labels on each sector of the pie chart show the contribution in both absolute value [$\mu g/m^3$] and percentage.

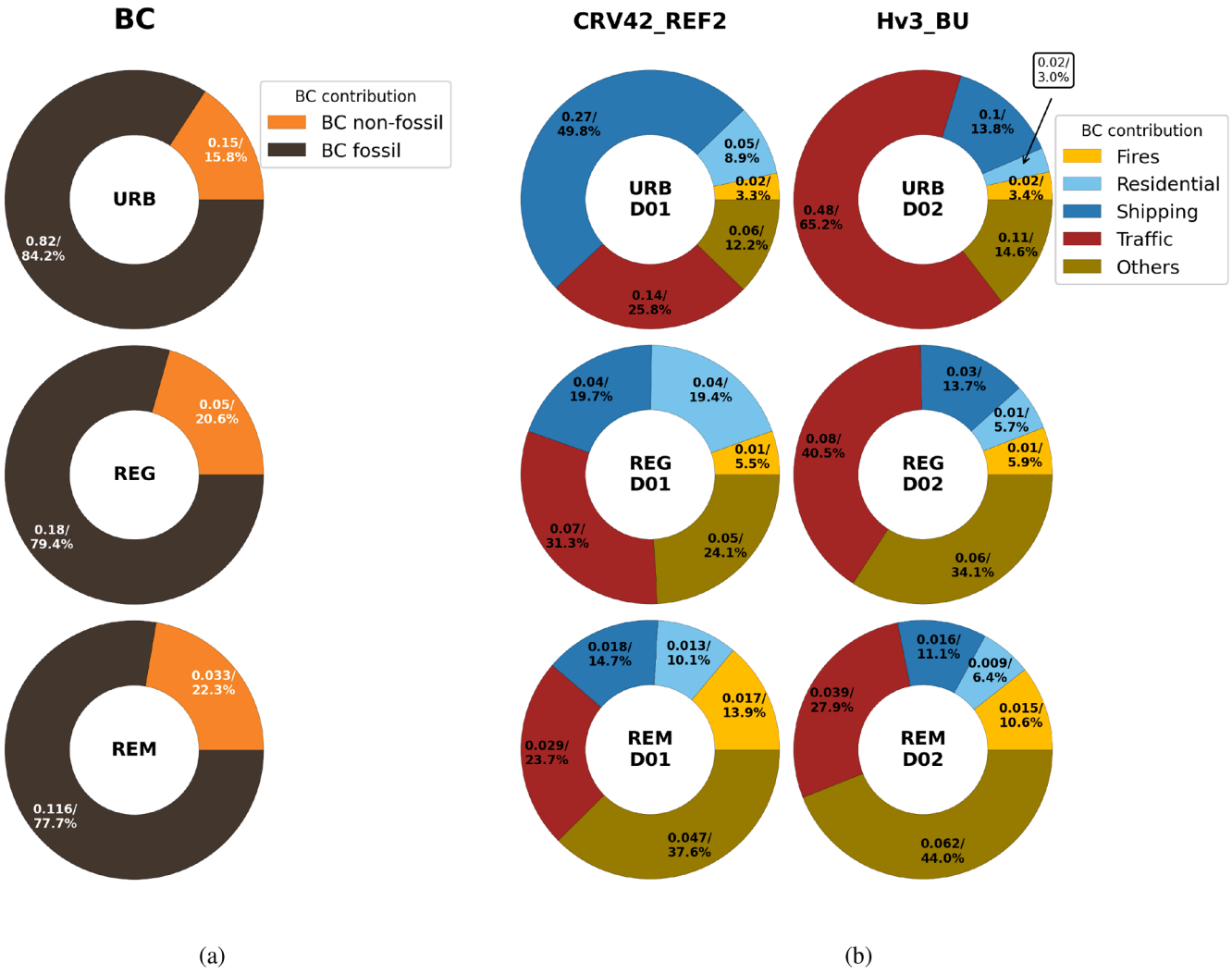

Fig. 7. Similar to Fig. 6 but for July month.

and agricultural waste burning. There is no direct equivalence between the *fossil/non-fossil* contribution quantified by observations and the model tags. Fossil emissions in the model runs includes *traffic* tag, *shipping* tag, but also part of *others* which considers contributions from public power, industry, aviation, off-road, and agricultural machinery. As shown in Fig. 3 and Fig. S1, the contribution of *others* emission sources is $< 6\%$ of total CA emissions for January and July. We thus consider that the *fossil* contribution derived from observations is closely related to *traffic* tag plus *shipping* tag plus *others* tag of the model. On the other hand, *non-fossil* sources in the model tags are mainly considered by *residential* and *fires* tags.

In this sense, the comparison between model and measurements is used as an indication of how the model characterizes the main source contributions, but has relevant uncertainties in both model and observational aspects.

Based on the observations (Figs. 6a and 7a), the most significant contributors to BC concentrations were fossil sources, with higher relative contributions in January at URB (0.66 $\mu g/m^3$/ 78.8%) compared to REG (0.06 $\mu g/m^3$/ 52.3%) and REM (0.02 $\mu g/m^3$/ 59.6%) due to higher biomass burning emissions (e.g., agricultural waste burning) in winter at these regional/remote sites compared to URB. In July, due to the lower use of biomass in the study area, fossil contributions to BC were similar at all three sites (77.7 −84.2%), although the concentrations were eight times greater in URB (0.82 $\mu g/m^3$) than REG and REM sites ($\sim$ 0.1 $\mu g/m^3$). Moreover, this similarity in relative terms could be also due to the atmospheric dynamics typical of the region in summer that favour the dispersion of pollutants over the region. The *fossil* and *non-fossil* contributions for URB and REG reported in Figs. 6a and 7a are consistent with the results from Minguillón et al. (2011), where 14C analysis was used for EC source apportionment. Specifically, Minguillón et al. (2011) found that at URB, on average, 87% and 91% of the EC in winter and summer, respectively, had a fossil origin, whereas at REG, these fractions were 66% and 79%, respectively.

The analysis of the model results reveals a significant under-representation of *traffic* in CRV42_REF2 (D01) for URB site, as illustrated in Figs. 6b and 7b. In particular, URB appears to be dominated by on-road *traffic* emissions which contribute significantly to the high observed *fossil* contribution 78.8% (0.66 $\mu g/m^3$) in January and 84.2% (0.82 $\mu g/m^3$) in July). However, D01 model results underestimate *traffic* influence, with a contribution of only 18.5% in January and 25.8% in July (0.14 $\mu g/m^3$ for both months). The under-representation of the observed *fossil* contribution by D01 remains in January even if we add the contribution from both *shipping* (0.15 $\mu g/m^3$/ 19.5%) and *others* (0.04 $\mu g/m^3$/ 4.6%) to *traffic* in URB, 42.6%. However, it reduces significantly in July mainly due to the increased role of *shipping* (0.27 $\mu g/m^3$/ 49.8% in URB).

Conversely, we find that the *residential* contribution in URB (0.43 $\mu g/m^3$/ 56.7%) is overestimated in January using CRV42_REF2 (D01) compared to observed *non-fossil* contribution of 21.2% (0.18 $\mu g/m^3$). Again, much better agreement is identified in July (not

just considering *residential* but *fires*).

Regarding D02 (using Hv3_BU emissions), our results show good agreement with observations, with the *fossil* contribution in URB to BC ranging from 70% to 80% in both January and July. This agreement is achieved by considering that mainly *traffic* plus *shipping* (76.5% and 79% in January and July) explain the observed *fossil* contribution (78.8% and 84.2%). Additionally, the agreement with observations improves if we consider that a fraction of *others* is a fossil source. While both CRV42_REF2 and Hv3_BU inventories show consistency in total PM emissions, as depicted in Fig. 3, their sector contribution significantly differ. According to CRV42_REF2, the *residential* sector (56.7% in January) and the *shipping* sector (49.8% in July) are specifically responsible for a substantial amount of BC concentrations. However, Hv3_BU and observational data point to a stronger contribution from the *traffic* sector, estimated at 65–70%. The use of detailed databases for Spain within Hv3_BU contributes to the precision and refinement of the emission estimates. This granularity and detail in emission generation might be one of the key reasons behind the uncertainties observed in *traffic*, *residential*, and *shipping* emissions between CRV42_REF2 and Hv3_BU.

Note that such discrepancies are not attributed to the model resolution but the underlying emissions as shown in Fig. S3, Fig. S5 and Fig. S6.

Consistent with the emissions, both the observations and model results indicate a higher contribution to BC from non-fossil sources at REG and REM compared to URB, and especially in January. Additionally, the model captures the contribution of biomass burning sources, which is particularly evident in REM where the *fires* contribution increases. This is consistent with the higher emissions of biomass burning from agricultural waste during winter and wildfires during summer, as well as the greater distance from fossil sources of BC at these regional/remote sites. The agreement between the observations and model was satisfactory at both the regional and remote levels (REG and REM) where a higher *non-fossil* contribution to BC was observed. In July, the contribution sectors gave more consistent results between the two inventories in both absolute values and percentage.

Overall, considering that the BC concentrations in URB were well reproduced by the model, as shown previously by Run-4 in Fig. 5, we suggest that the spatial distribution of *residential* emissions based on population density and wood availability compensates for the underestimation of *traffic* emissions in the CRV42_REF2 emission inventory, particularly relevant during wintertime. This issue is further illustrated in Fig. S5 and Fig. S6.

It is important to note that the relative contributions to BC from fossil and non-fossil sources were subject to a high degree of uncertainty in both the experimental and modeling aspects of the study. Nevertheless, the model clearly captured the relative increase of non-fossil sources to BC when moving from the urban level to the regional/remote level. These comparisons highlight the advantages of using bottom-up approaches that incorporate specific information about a region, and the need to revise the spatial distribution of *residential* emissions in continental-scale inventories like CAMS-REG.

3.4. Organic Aerosol surface concentration and source contribution

In this section, we discuss the OA results of Run-4 and their comparison with Q-ACSM measurements available in URB, and with 24 h filter measurements available at the three sites. On a second step, the source contribution to OA concentrations is analyzed in URB site based on Run-5 and availability of measurements for the apportionment technique.

Table 4 presents the performance indicator metrics for OA during the year 2018, where the 24 h filter data was used in all three stations to maintain consistency. To compare the OA simulated by the model with OC, we applied a ratio of OM:OC of 1.7 in URB and 2.1 in REG and REM (see Section 2.2.4 for details). Among the three domains, D03 performed the best in URB, meeting the benchmark throughout the year with a NMB of 1.12%, NME of 21.78%, and a good correlation coefficient ($PCC = 0.75$). Good values for FB $< \pm 6\%$ and FAC2 $> 90\%$ confirmed the model's excellent performance in D03. In seasonal analysis, D03 also showed excellent agreement during spring (refer to Table S4). However, all over the year and especially in winter, D01 statistics worsened significantly compared to D02 and D03, which is likely due to the spatial distribution of emissions and the speciation applied in the CRV42_REF2 emission inventory (see Table 2 and Section 3.1).

In REG, both D02 and D03 met the benchmark criteria, with NMB of -36.38% for D02 and -43.12% for D03 and NME of 40.38% for D02 and 44.58% for D03. PCCs for D02 and D03 were relatively high, indicating good temporal variability in the model. However, there was a general underestimation in summer (see Table S4 for all three domains), suggesting an underestimation of biogenic secondary organic aerosol production in the region as identified previously. D01 showed a systematic overestimation during the winter season, consistent with results in URB (see Table S4).

Table 4 demonstrates that the model performance decreases as the distance from urban areas increases, with fewer metrics meeting the goal or criteria benchmarks. Moreover, Fig. 8 and Table 4 illustrate the positive effect of the domain resolution and provide further insights into the combined impact of resolution and location of the considered site. As presented in Table S4, the performance of the REM site exhibits seasonal variations. During the MAM season, the site displays an enhanced correlation between predicted and observed values; however, the underprediction of OA concentrations persists throughout all seasons. In contrast, the JJA season exhibits the lowest prediction accuracy, with a smaller proportion of predictions falling within a factor of 2 of the observations compared to other seasons.

Fig. 8 displays the time series of daily average concentrations of organic aerosol (OA) in the three sites (URB, REG, and REM) for the year 2018. The black line in Fig. 8a represents data obtained from Q-ACSM instrument (URB site), while blue triangles represent OA data derived from 24-h filters (URB, REG, and REM), assuming same ratio of organic matter to organic carbon (OM:OC) as indicated before. The results for URB (Fig. 8a) indicate a consistent pattern of OA concentrations throughout the year, except for winter when the first domain overestimates the OA concentrations. This behavior can largely be attributed to the spatial distribution of the residential emissions as discussed in Section 3.2, which can affect the accuracy of the model. Overall, D02 and D03 results are in excellent agreement with the observations.

In Fig. 8b, the seasonality of OA concentrations in REG is presented. As previously mentioned, REG is a measuring station located in a regional background surrounded by vegetation and situated in a natural park. The transport of pollutants from the URB metropolitan area towards REG is facilitated by the sea breeze circulation, particularly during spring and summer. The results show that the highest concentrations of OA occur during the hot months (JJA), with an average value of 4.56 $\mu g/m^3$. In contrast, the lowest concentrations of OA are observed during the coldest months (DJF), with the model reporting average values of 5.72 $\mu g/m^3$, 1.5 $\mu g/m^3$, and 1 $\mu g/m^3$ for D01, D02 and D03, respectively. The observations, on the other hand, indicate an average value of $2\mu g/m^3$.

Model underestimations during summer could be attributed to limited biogenic SOA production in the model scheme (no NOx sensitivity in biogenic SOA yields). Overall, the domains with high resolution exhibit a similar behavior throughout the period, with correlations > 0.8, suggesting that the model captures OA variability at the regional level reasonably well.

At the REM station, a remote background site with low direct human influence, the results of the three model domains remain consistent throughout the year, as shown in Fig. 8c. Although there is some underestimation during JJA and September, the model accurately captures the variability of OA level concentrations during the rest of the period.

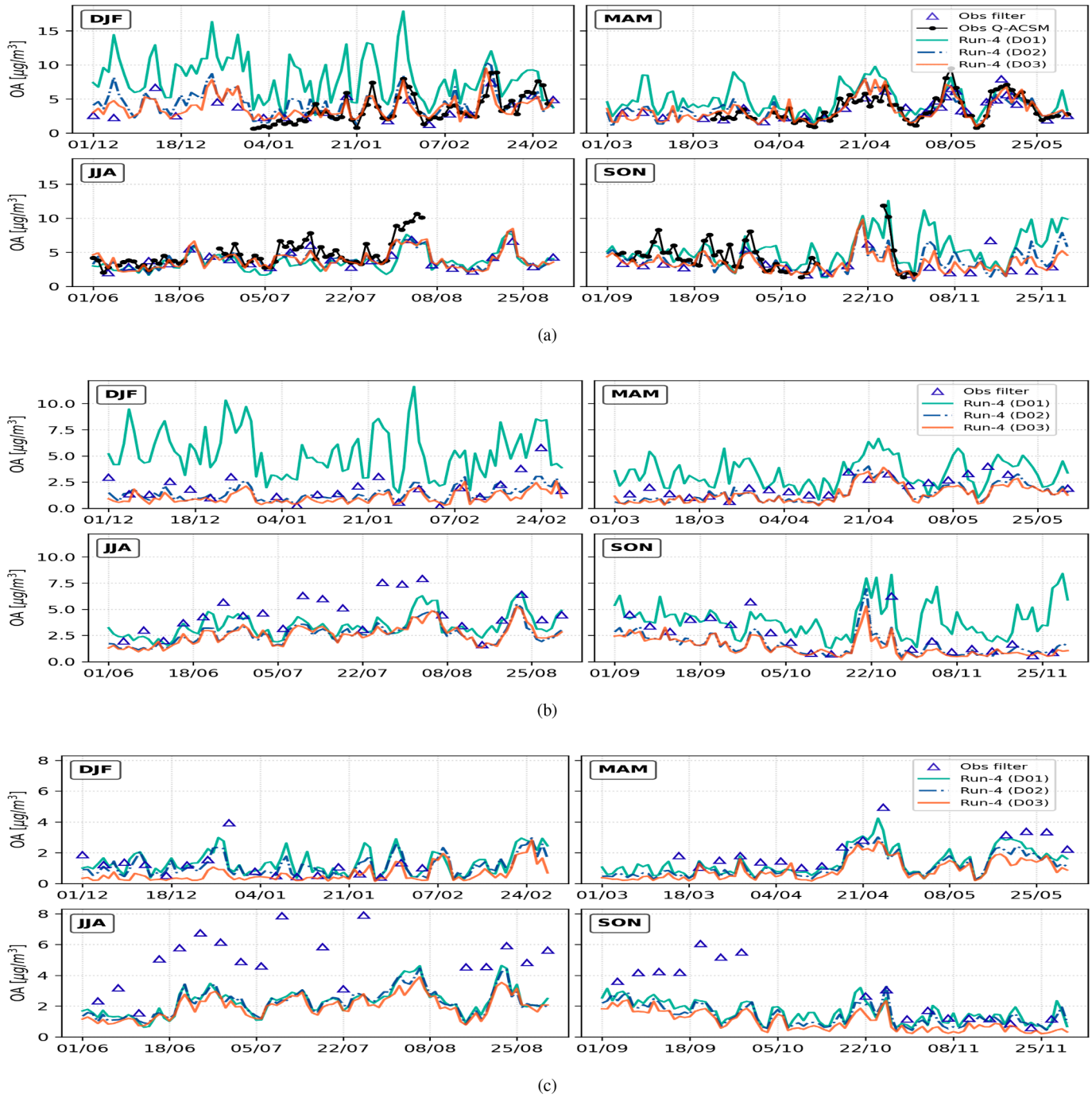

Fig. 8. Time series of daily-average OA concentrations at (a) URB, (b) REG, and (c) REM sites for 2018 (Q-ACSM observations black line, 24-h filters observations blue triangles, Run-4 D01 green line, Run-4 D02 dashed-dotted blue line, and Run-4 D03 orange line). Panels grouped in December-January-February (DJF), March-April-May (MAM), June-July-August (JJA), and September-October-November (SON).

The correlation coefficients for domains D01, D02, and D03 are 0.6, 0.7, and 0.8, respectively.

In order to quantify the apportionment to OA concentrations, we compare results of Run-5 (Table 3) against the OA sources identified by the Q-ACSM instrument (Section 2.2.3) only available in URB site. Similarly to the BC analysis, there is no direct match between the contributions derived from observations and the model. For sake of simplicity, we assume that Q-ACSM HOA source is a proxy of primary organic *traffic* contribution derived from the model (*POA Traffic*), COA plus BBOA is close to primary *residential* emissions (*POA Residential*) and LO-OOA and MO-OOA describes SOA contribution. Fig. 9 presents the monthly mean contribution (absolute values and percentage) of sources derived from Q-ACSM and Run-5 (D01 and D02 results at URB) to OA concentration for January and July.

In January, observations indicate that SOA is the main contributor (mean concentration of 1.65$\mu g/m^3$), accounting for 60% of total OA, followed by the *residential* (25%) and *traffic* (15%) sectors. Model results suggest a better representation of *residential* and *traffic* contributions by the local Hv3_BU inventory when compared with the observations. Here, the hypothesis on the limitations highlighted previously in the description of *residential* sources in D01 is confirmed (a factor x10 of overestimation compared with observations). Such a large difference should be considered when comparing the contributions of other sources which might look far from the observational results in percentage but

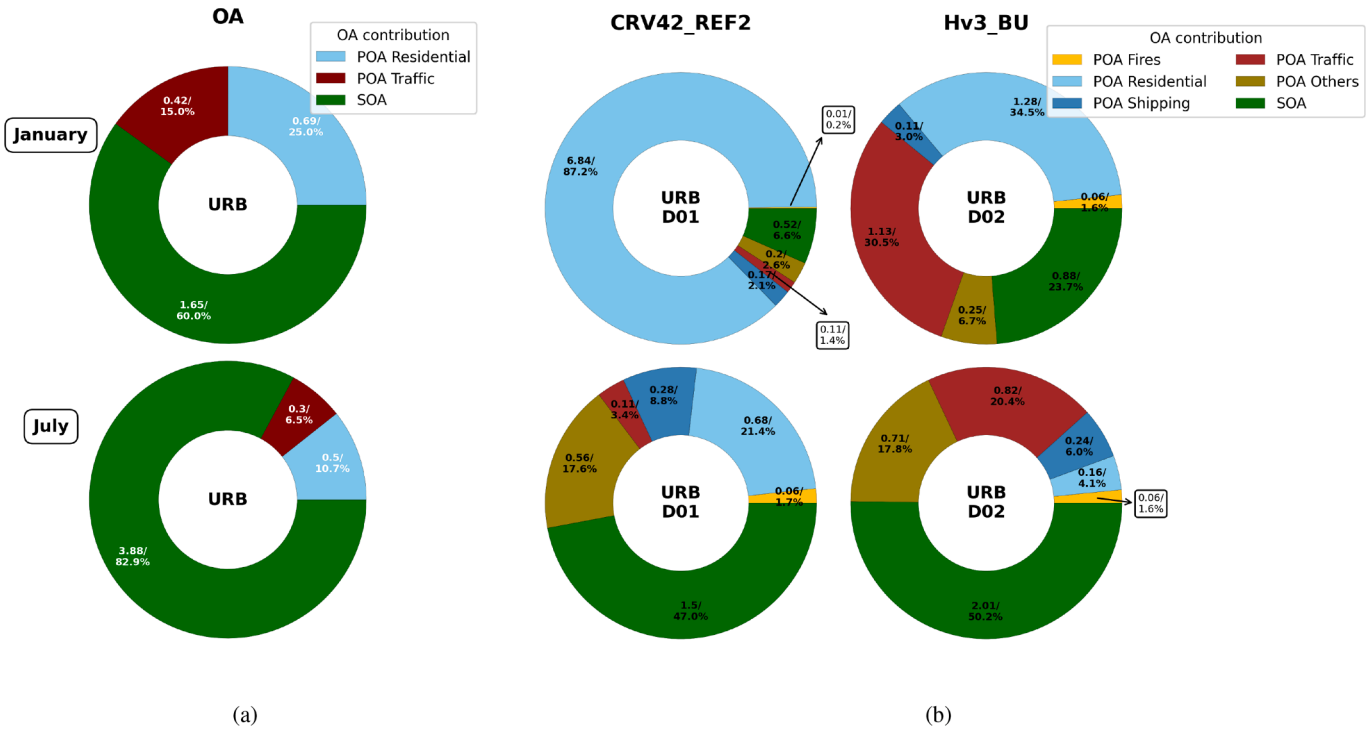

(a) (b)

Fig. 9. The monthly mean contribution of OA surface concentration from emission sources for January and July 2018 at URB site derived from (a) Q-ACSM observations and (b) the MONARCH Run-5 simulation. The columns represent the model results for D01 and D02, and the colors indicate the different sources tagged. The labels on each sector of the pie chart show the contribution in both absolute value [$\mu g/m^3$] and percentage.

closer in absolute value (e.g., SOA contribution).

The comparison between results obtained with CRV42_REF2 (D01) and Hv3_BU (D02) inventories reveals significant discrepancies in the contributions from *residential* and *traffic*. The contribution of *residential* emissions in CRV42_REF2 (6.84$\mu g/m^3$/ 87.2%) is significantly higher than in Hv3_BU (1.28$\mu g/m^3$/ 34.5%), which could be due to differences in emission assumptions about spatial distribution (see discussion in Section 3.1 and Section 3.2). On the contrary, *traffic* emissions in CRV42_REF2 explains a significantly lower fraction of total OA (0.11$\mu g/m^3$/ 1.4%) than Hv3_BU (1.13$\mu g/m^3$/ 30.58%), likely due to differences in activity data and spatial distribution of total PM emissions between inventories. A closer agreement is found in the SOA contribution between runs, with slightly higher concentrations obtained in D02 (0.88$\mu g/m^3$) than in D01 (0.52$\mu g/m^3$).

Finally, the contributions of *shipping*, *fires*, and *others* sources are relatively small in both inventories. Although they are unlikely to have a significant impact on OA concentrations in URB during January, they could still be important in specific areas, such as near ports or areas with high wildfire risk.

All in all, the evaluation with observations suggests a better agreement using the Hv3_BU inventory (D02) than D01. However, the relatively low formation of SOA in the MONARCH model may indicate the need for a more refined scheme as some of the SOA simulated in URB might be apportioned as primary sources instead of secondary production (i.e., combustion sources). it is important to highlight that the contributions derived from the Q-ACSM are not exempt from uncertainty, reaching errors up to $\pm$ 40% for some SOA species as previously mentioned in Section 2.2.3.

In relation to the summer period, results derived from both inventories reveal that SOA constitutes the largest contributor to OA in URB. While the proportion of SOA in D02 slightly exceeds that in D01, 50.2% and 47% respectively, significant discrepancies emerge in the contributions from *traffic* and *residential* sectors between the two domains, when compared to observational data (akin to the pattern observed in January). Specifically, in the CRV42_REF2 inventory, *residential* sources contribute 0.68$\mu g/m^3$ to OA, accounting for 21.4%, while in the Hv3_BU inventory, the contribution is significantly lower at 0.16$\mu g/m^3$, representing just 4.1%. On the contrary, the Hv3_BU inventory assigns a greater proportion of 20.4% (0.82$\mu g/m^3$) to *traffic* sources, in comparison to the CRV42_REF2 inventory's modest 0.11$\mu g/m^3$ (3.4%). Despite this, contributions from sources like *fires* and *shipping* appear to have a limited influence on OA during July. It is worth noting that a distinct sector categorized as *others* makes a non-negligible contribution to OA and would require further investigation.

The observations in URB underscore SOA as the dominant OA contributor, accounting for more than 80% of the total OA during summer, likely due to photochemical activity. However, the modeled results from both domains fall short in replicating the SOA contribution. This discrepancy suggests that the model's simplified SOA scheme might not capture the intricate atmospheric chemistry or the impact of photochemistry on SOA formation. Interestingly, the model's resolution shows no substantial differences on the results, implying that other factors such as chemistry scheme, emissions, or meteorological inputs might be more critical on model performance enhancement. Further investigations are necessary to discern the caues of the disparities between observations and modeling outputs, while advancing the representation of SOA formation in models.

In summary, there are significant discrepancies between the results obtained with the Hv3_BU and CRV42_REF2 inventories for summer and winter months in URB. As expected, contributions from *residential* sources intensify in colder months and SOA sources prevail in summer, variations effectively reproduced by the model using detailed emission inputs.

All in all, the source apportionment of OA is intricate due to the complexity in simulating SOA production, the treatment of SOA precursors (different volatilities based on emission sources) and the need for precise tagging methods.

4. Conclusions

In this study, we investigated the uncertainties in the representation of carbonaceous aerosols in a Mediterranean region and their source contributions (i.e., traffic, RWC, shipping, fires) derived from both measurements and modelling techniques. Annual simulations of year 2018 using the MONARCH model with different emission inventories (CRV42, CRV42_REF2, and Hv3_BU) were analyzed. CRV42 and CRV42_REF2 are two versions of the European-scale emission inventory CAMS-REG_v4, the latter being a science version using a consistent approach for RWC PM emissions. The third inventory used in this work is a bottom-up inventory for Spain produced with the HERMESv3_BU emission model (Hv3_BU). We examined the impact of model resolution by using two standard configurations: one with a single domain covering Europe and part of North Africa at a horizontal resolution of ~ 20 km and another with a nested configuration featuring three domains at horizontal resolutions of ~ 20 km, ~ 5 km, and ~ 1 km (first two used for the source apportionment analysis). We compared model results with observations measurements performed by EGAR-IDAEA group at three supersites of NE Spain representing different environments (URB urban, REG regional and REM remote), those measurements includes MAAP for BC and Filter and Q-ACSM for OA.

The study showed that the MONARCH model effectively captured BC concentrations in the three sites, although there were some issues during winter. While OA concentrations were reasonably well modeled, SOA was underestimated (particularly from biogenic sources). Additionally, limitations were identified in the CAMS inventories, such as an over-representation of *residential* emissions in the urban site at expenses of a lack of *traffic* emissions. However, using the condensable fraction in CRV42_REF2 and Hv3_BU in the *residential* sector significantly improved the model's performance, particularly for BC concentrations, by identifying the critical role of PM speciation. Our study revealed that BC concentrations were overestimated with the CRV42 inventory, and a monthly V-shape temporal distribution was simulated in URB and REG throughout the year not correctly reproducing the observations. This issue improved using Hv3_BU emissions.

The MONARCH model was able to accurately describe the *non-fossil* and *fossil* contributions to BC in URB/REG using the Hv3_BU inventory. *Shipping* and *residential* sources of BC were found to be significant contributors in URB during summer and winter respectively, while *traffic* emissions dominated overall. Emissions were found to be consistent in total PM between CRV42_REF2 and Hv3_BU. However, CRV42_REF2 over-represented the contribution of *residential* (winter) and *shipping* (summer) compared with Hv3_BU or observations.

Additionally, the study found that OA was overestimated in URB/REG during winter and spring with the CRV42_REF2 inventory, and, similarly to CRV42 for BC, a well-defined V-shape was identified in simulated OA concentrations throughout the year in the three environments. Again, this feature was not observed in the measurements and the best match was obtained using Hv3_BU. A feature that highlights the critical need of accurate profiles for temporal distribution of emissions. The model's performance was limited in remote areas such as REM due to the low concentration of observations, which were below the limit of detection, and the complexity of the topography.

The work has identified some limitations in both measurement and modeling approaches. The BC source apportionment from the Sandradewi model has a rather high uncertainty (not less than 20%) due to specific assumptions in the model as the Absorption Angstrom Exponents (AAE) chosen for fossil and non-fossil sources and the assumption of equal MAC of BC emitted from these two source categories. Moreover, the definition of fossil and non-fossil BC sources from the Sandradewi model, and consequently the direct comparison with chemistry models, can be complicated. In fact, the physical properties of BC particles emitted by combustion sources strongly depend on the efficiency of burning conditions. For example, it has been observed that *shipping* emissions, despite the fact that vessels burn fossil fuel, can enter in the non-fossil category in the Sandradewi model due to the high AAE observed when vessels burn high sulfur content heavy fuel oil. Similarly, wood burning derived aerosols can have a low AAE (close to the AAE of *traffic* emisisons) if modern masonry heater are used (Helin et al., 2021). Regarding emission inventories, the spatio-temporal disaggregation of emission sources remains a challenging topic for modeling studies. Although emission inventories might agree on the total PM annual emissions, significant differences arise when source contribution is analyzed. Despite the well-established nature of certain sectors, such as traffic, notable uncertainties persist on top of the significant challenges in understanding complex sources like RWC. Moreover, there are some overestimation of specific sectors due to a lack of reliable information (e.g., agricultural machinery emissions). Finally, chemical transport models are not free from limitations. In our study, a simple SOA scheme has been adopted simplifying the analysis of results and providing a consistent method for source attribution. However, the model's limitations in reproducing the contribution of SOA, particularly during the summer, were highlighted likely due to the limited biogenic SOA production. It is important to acknowledge the complexities of modeling OA, specifically SOA. Zhang et al. (2013) and Basla et al. (2022) demonstrate the effectiveness of Volatility Basis Set (VBS) approach, emphasizing the volatility of primary organic aerosols and the aging of semi-volatile compounds. However, Fountoukis et al. (2016) expose a limitation in wintertime SOA modeling, suggesting unaccounted SOA formation processes. Meanwhile, Meroni et al. (2017) and Ciarelli et al. (2016) underscore the model sensitivity to OA schemes, with underpredictions in PM concentrations and SOA. The simplified scheme designed by Pai et al. (2020) used in this work provides a balanced approach to minimize the overall OA bias while maintaining similar correlation compared with a VBS approach. These findings and our results stress the need for refined modeling approaches and accurate emission inventories for better OA representation.

Despite the limitations identified in the study, the results provide valuable insights into the effectiveness of the use of a chemistry model like MONARCH in simulating BC/OA concentrations in NE Spain. The importance of speciation and refined treatment of low-volatile condensable emissions are emphasized as key factors in improving the model's performance. These findings underscore the need for continued efforts to refine the underlying emission inventories and modeling techniques to better understand and mitigate the impacts of air pollution on human health and the environment.

Authors contributions. HN, MP and OJ contributed to the conceptualization, design, and the analysis of the work. HN, MG, SE, CT contributed to the emissions processing. HN contributed to conducting MONARCH runs and data processing. MP, MV, JYD, CR, NP, AA, XQ contributed to the provision of measurement data. OJ, MP, XQ, AA contributed to acquiring funding. HN, MP and OJ prepared the manuscript with contributions from all co-authors.

Declaration of Competing Interest

The authors declare that they have no known competing financial interests or personal relationships that could have appeared to influence the work reported in this paper.

Data availability

Data will be made available on request.

Acknowledgements

Hector Navarro-Barboza acknowledges financial support from the Spanish Ministry for Science and Innovation (FPI PRE2018-084988 financed by MCIN/AEI/10.13039/501100011033 and by ESF Investing in your future). The research leading to these results has received funding from the Ministerio de Ciencia, Innovación y Universidades as

part of the BROWNING project (Grant No. RTI2018-099894-B-I00 funded by MCIN/AEI/10.13039/501100011033 and by "ERDF A way of making Europe") and the Ministerio de Asuntos Económicos y Transformación Digital, Gobierno de España as part of the CAIAC project (Grant No. PID2019-108990 PB-100). This project has received funding from the Agencia Estatal Consejo Superior de Investigaciones Científicas (CSIC) under the Project 202030E261, and the Generalitat de Catalunya, by AGAUR (2021 SGR 00447) and the Direcció General de Qualitat Ambiental i Canvi Climàtic (DGQACC). This project has also received funding from the European Union's Horizon Europe research and innovation programme under the RI-URBANs project (grant agreement No 101036245). IDAEA-CSIC is a Centre of Excellence Severo Ochoa (Spanish Ministry of Science and Innovation, Grant No. CEX2018-000794-S).

BSC researchers thankfully acknowledge the computer resources at Marenostrum and the technical support provided by Barcelona Supercomputing Center (RES-AECT-2021–1-0027, RES-AECT-2021–2-0001).

Appendix A. Supplementary data

Supplementary data to this article can be found online at https://doi.org/10.1016/j.envint.2023.108252.

References

Aas, W., Tsyro, S., Bieber, E., Bergström, R., Ceburnis, D., Ellermann, T., Fagerli, H., Frölich, M., Gehrig, R., Makkonen, U., et al., 2012. Lessons learnt from the first EMEP intensive measurement periods. Atmos. Chem. Phys. 12, 8073–8094.

Amato, F., Karanasiou, A., Moreno, T., Alastuey, A., Orza, J., Lumbreras, J., Borge, R., Boldo, E., Linares, C., Querol, X., 2012. Emission factors from road dust resuspension in a Mediterranean freeway. Atmos. Environ. 61, 580–587.

Athanasopoulou, E., Speyer, O., Brunner, D., Vogel, H., Vogel, B., Mihalopoulos, N., Gerasopoulos, E., 2017. Changes in domestic heating fuel use in Greece: effects on atmospheric chemistry and radiation. Atmos. Chem. Phys. 17, 10597–10618. https://doi.org/10.5194/acp-17-10597-2017.

Badia, A., Jorba, O., 2015. Gas-phase evaluation of the online NMMB/BSC-CTM model over Europe for 2010 in the framework of the AQMEII-Phase2 project. Atmos. Environ. 115, 657–669.

Badia, A., Jorba, O., Voulgarakis, A., Dabdub, D., Pérez García-Pando, C., Hilboll, A., Gonçalves Ageitos, M., Zavisa, J., 2017. Description and evaluation of the Multiscale Online Nonhydrostatic AtmospheRe CHemistry model (NMMB-MONARCH) version 1.0: gas-phase chemistry at global scale. Geoscient. Model Develop. 10, 609–638.

Basla, B., Agresti, V., Balzarini, A., Giani, P., Pirovano, G., Gilardoni, S., Paglione, M., Colombi, C., Belis, C.A., Poluzzi, V., et al., 2022. Simulations of organic aerosol with CAMx over the Po Valley during the summer season. Atmosphere 13, 1996.

Bell, M.L., Davis, D.L., Gouveia, N., Borja-Aburto, V.H., Cifuentes, L.A., 2006. The avoidable health effects of air pollution in three Latin American cities: Santiago, Sao Paulo, and Mexico City. Environ. Res. 100, 431–440.

Bergström, R., 2020. How should condensables be included in PM emission inventories reported to EMEP/CLRTAP? EMEP 1–72.

Boylan, J.W., Russell, A.G., 2006. PM and light extinction model performance metrics, goals, and criteria for three-dimensional air quality models. Atmos. Environ. 40, 4946–4959.

Brines, M., Dall'Osto, M., Beddows, D., Harrison, R.M., Querol, X., 2014. Simplifying aerosol size distributions modes simultaneously detected at four monitoring sites during SAPUSS. Atmos. Chem. Phys. 14, 2973–2986.

Cavalli, F., Viana, M., Yttri, K.E., Genberg, J., Putaud, J.-P., 2010. Toward a standardised thermal-optical protocol for measuring atmospheric organic and elemental carbon: the EUSAAR protocol. Atmos. Meas. Tech. 3, 79–89. https://doi.org/10.5194/amt-3-79-2010. URL https://amt.copernicus.org/articles/3/79/2010/.

Chafe, Z., Brauer, M., Héroux, M.-E., Klimont, Z., Lanki, T., Salonen, R.O., Smith, K.R., 2015. Residential heating with wood and coal. In: Health Impacts and Policy Options in Europe and North America.

Chang, J.C., Hanna, S.R., 2004. Air quality model performance evaluation. Meteorol. Atmos. Phys. 87, 167–196.

Chen, G., Jin, Z., Li, S., Jin, X., Tong, S., Liu, S., Yang, Y., Huang, H., Guo, Y., 2018. Early life exposure to particulate matter air pollution (PM1, PM2. 5 and PM10) and autism in Shanghai, China: A case-control study. Environ. Int. 121, 1121–1127.

Chen, G., Sosedova, Y., Canonaco, F., Fröhlich, R., Tobler, A., Vlachou, A., Daellenbach, K.R., Bozzetti, C., Hueglin, C., Graf, P., et al., 2021. Time-dependent source apportionment of submicron organic aerosol for a rural site in an alpine valley using a rolling positive matrix factorisation (PMF) window. Atmos. Chem. Phys. 21, 15 081–15 101.

Chen, G., Canonaco, F., Tobler, A., Aas, W., Alastuey, A., Allan, J., Atabakhsh, S., Aurela, M., Baltensperger, U., Bougiatioti, A., et al., 2022. European aerosol phenomenology- 8: Harmonised source apportionment of organic aerosol using 22 Year-long ACSM/AMS datasets. Environ. Int. 166, 107 325.

Chin, M., Ginoux, P., Kinne, S., Torres, O., Holben, B.N., Duncan, B.N., Martin, R.V., Logan, J.A., Higurashi, A., Nakajima, T., 2002. Tropospheric aerosol optical thickness from the GOCART model and comparisons with satellite and Sun photometer measurements. J. Atmos. Sci. 59, 461–483.

Ciarelli, G., Aksoyoglu, S., Crippa, M., Jimenez, J.-L, Nemitz, E., Sellegri, K., Äijälä, M., Carbone, S., Mohr, C., O'Dowd, C., Poulain, L., Baltensperger, U., et al., 2016. Evaluation of European air quality modelled by CAMx including the volatility basis set scheme. Atmos. Chem. Phys. 16, 10313–10332. https://doi.org/10.5194/acp-16-10313-2016.

Copernicus: State-of-the-European-climate: February 2018, https://surfobs.climate.copernicus.eu/stateofthe climate/february2018.php, [Online; accessed 15-September-2022], 2018.

Crippa, M., Guizzardi, D., Muntean, M., Schaaf, E., Dentener, F., Van Aardenne, J.A., Monni, S., Doering, U., Olivier, J.G., Pagliari, V., et al., 2018. Gridded emissions of air pollutants for the period 1970–2012 within EDGAR v4. 3.2. Earth Syst. Sci. Data 10, 1987–2013.

Denier Van Der Gon, H., Bergström, R., Fountoukis, C., Johansson, C., Pandis, S., Simpson, D., Visschedijk, A.J., 2015. Particulate emissions from residential wood combustion in Europe–revised estimates and an evaluation. Atmos. Chem. Phys. 15, 6503–6519.

Drinovec, L., Močnik, G., Zotter, P., Prévôt, A., Ruckstuhl, C., Coz, E., Rupakheti, M., Sciare, J., Müller, T., Wiedensohler, A., et al., 2015. The dual-spot Aethalometer: an improved measurement of aerosol black carbon with real-time loading compensation. Atmos. Meas. Tech. 8, 1965–1979.

Ealo, M., Alastuey, A., Ripoll, A., Pérez, N., Minguillón, M.C., Querol, X., Pandolfi, M., 2016. Detection of Saharan dust and biomass burning events using near-real-time intensive aerosol optical properties in the north-western Mediterranean. Atmos. Chem. Phys. 16, 12 567.

Ealo, M., Alastuey, A., Pérez, N., Ripoll, A., Querol, X., Pandolfi, M., 2018. Impact of aerosol particle sources on optical properties in urban, regional and remote areas in the north-western Mediterranean. Atmos. Chem. Phys. 18, 1149–1169.

Echalar, F., Artaxo, P., Martins, J.V., Yamasoe, M., Gerab, F., Maenhaut, W., Holben, B., 1998. Long-term monitoring of atmospheric aerosols in the Amazon Basin: Source identification and apportionment. J. Geophys. Res.: Atmos. 103, 31 849–31 864.

EEA: Air quality in Europe 2022, Technical report, EEA, URL https://www.eea.europa.eu/publications/air-quality-in-europe-2022/, 2022.

EMEP and EEA: EMEP/EEA Air Pollutant Emission Inventory Guidebook 2019: Technical Guidance to Prepare National Emission Inventories, Tech. rep., European Environment Agency, URL https://www.eea.europa.eu/publications/emep-eea-guidebook-2019, 2019.

Emery, C., Liu, Z., Russell, A.G., Odman, M.T., Yarwood, G., Kumar, N., 2017. Recommendations on statistics and benchmarks to assess photochemical model performance. J. Air Waste Manage. Assoc. 67, 582–598.

Fagerli, H., Tsyro, S., Jonson, J.E., Nyíri, Á., Gauss, M., Simpson, D., Wind, P., Benetictow, A., Klein, H., Mortier, A., et al., 2019. Transboundary particulate matter, photo-oxidants, acidifying and eutrophying components.

Flemming, J., Huijnen, V., Arteta, J., Bechtold, P., Beljaars, A., Blechschmidt, A.-M., Diamantakis, M., Engelen, R.J., Gaudel, A., Inness, A., et al., 2015. Tropospheric chemistry in the Integrated Forecasting System of ECMWF. Geoscient. Model Develop. 8, 975–1003.

Florczyk, A.J., Corbane, C., Ehrlich, D., Freire, S., Kemper, T., Maffenini, L., Melchiorri, M., Pesaresi, M., Politis, P., Schiavina, M., Sabo, F., Zanchetta, L., 2019. GHSL Data Package 2019, EUR 29788EN. Publications Office of the European Union, Luxembourg. https://doi.org/10.2760/062975, 978-92-76-08725-0, JRC117104.

Foster, A., Kumar, N., 2011. Health effects of air quality regulations in Delhi. India, Atmos. Environ. 45, 1675–1683.

Fountoukis, C., Megaritis, A.G., Skyllakou, K., Charalampidis, P.E., Denier van der Gon, H.A., Crippa, M., Prévôt, A.S., Fachinger, F., Wiedensohler, A., Pilinis, C., et al., 2016. Simulating the formation of carbonaceous aerosol in a European Megacity (Paris) during the MEGAPOLI summer and winter campaigns. Atmos. Chem. Phys. 16, 3727–3741.

Granier, C., Darras, S., van der Gon, H.D., Jana, D., Elguindi, N., Bo, G., Michael, G., Marc, G., Jalkanen, J.-P., Kuenen, J., et al., 2019. The Copernicus atmosphere monitoring service global and regional emissions (April 2019 version). Ph.D. thesis, Copernicus Atmosphere Monitoring Service.

Grythe, H., Lopez-Aparicio, S., Vogt, M., Vo Thanh, D., Hak, C., Halse, A.K., Hamer, P., Sousa Santos, G., 2019. The MetVed model: development and evaluation of emissions from residential wood combustion at high spatio-temporal resolution in Norway. Atmos. Chem. Phys. 19, 10 217–10 237.

Guenther, A., Karl, T., Harley, P., Wiedinmyer, C., Palmer, P.I., Geron, C., 2006. Estimates of global terrestrial isoprene emissions using MEGAN (Model of Emissions of Gases and Aerosols from Nature). Atmos. Chem. Phys. 6, 3181–3210. https://doi.org/10.5194/acp-6-3181-2006. URL https://acp.copernicus.org/articles/6/3181/2006/.

Guevara, M., Tena, C., Porquet, M., Jorba, O., Pérez García-Pando, C., 2019. HERMESv3, a stand-alone multi-scale atmospheric emission modelling framework–Part 1: global and regional module. Geoscient. Model Develop. 12, 1885–1907.

Guevara, M., Tena, C., Porquet, M., Jorba, O., Pérez García-Pando, C., 2020. HERMESv3, a stand-alone multi-scale atmospheric emission modelling framework–Part 2: The bottom–up module. Geoscient. Model Develop. (GMD) 13, 873–903.

Guevara, M., Jorba, O., Tena, C., Denier van der Gon, H., Kuenen, J., Elguindi, N., Darras, S., Granier, C., Pérez García-Pando, C., 2021. Copernicus Atmosphere Monitoring Service TEMPOral profiles (CAMS-TEMPO): global and European emission temporal profile maps for atmospheric chemistry modelling. Earth Syst. Sci. Data 13, 367–404. https://doi.org/10.5194/essd-13-367-2021. URL https://essd.copernicus.org/articles/13/367/2021/.

Guevara, M., Jorba, O., Tena, C., Denier van der Gon, H., Kuenen, J., Elguindi, N., Darras, S., Granier, C., Pérez García-Pando, C., 2021. Copernicus Atmosphere Monitoring Service TEMPOral profiles (CAMS-TEMPO): global and European emission temporal profile maps for atmospheric chemistry modelling. Earth Syst. Sci. Data 13, 367–404.

Hallquist, M., Wenger, J.C., Baltensperger, U., Rudich, Y., Simpson, D., Claeys, M., Dommen, J., Donahue, N., George, C., Goldstein, A., et al., 2009. The formation, properties and impact of secondary organic aerosol: current and emerging issues. Atmos. Chem. Phys. 9, 5155–5236.

Hanisch, F., Crowley, J.N., 2001. The heterogeneous reactivity of gaseous nitric acid on authentic mineral dust samples, and on individual mineral and clay mineral components. PCCP 3, 2474–2482.

Helin, A., Virkkula, A., Backman, J., Pirjola, L., Sippula, O., Aakko-Saksa, P., Väätäinen, S., Mylläri, F., Järvinen, A., Bloss, M., Jakobi, G., Karjalainen, P., Zimmermann, R., Jokiniemi, J., Saarikoski, S., Tissari, J., Rönkkö, T., Niemi, J.V., Timonen, H., 2021. Variation of absorption Ångström exponent in aerosols from different emission sources. J. Geophys. Res.: Atmos. 126 (10) https://doi.org/10.1029/2020JD034094 e2020JD034094.

Hitzenberger, R., Tohno, S., 2001. Comparison of black carbon (BC) aerosols in two urban areas–concentrations and size distributions. Atmos. Environ. 35, 2153–2167.

Jaeglé, L., Quinn, P., Bates, T., Alexander, B., Lin, J.-T., 2011. Global distribution of sea salt aerosols: new constraints from in situ and remote sensing observations. Atmos. Chem. Phys. 11, 3137–3157.

Janjic, Z., Gall, L., 2012. Scientific documentation of the NCEP nonhydrostatic multiscale model on the B grid (NMMB). Part 1 Dynamics. Tech. rep., National Center for Atmospheric Research.

Janjic, Z.I., Gerrity Jr, J., Nickovic, S., 2001. An alternative approach to nonhydrostatic modeling. Mon. Weather Rev. 129, 1164–1178.

Jimenez, J.L., Canagaratna, M., Donahue, N., Prevot, A., Zhang, Q., Kroll, J.H., DeCarlo, P.F., Allan, J.D., Coe, H., Ng, N., et al., 2009. Evolution of organic aerosols in the atmosphere. Science 326, 1525–1529.

Jorba, O., Dabdub, D., Blaszczak-Boxe, C., Pérez, C., Janjic, Z., Baldasano, J.M., Spada, M., Badia, A., Gonçalves, M., 2012. Potential significance of photoexcited NO2 on global air quality with the NMMB/BSC chemical transport model. J. Geophys. Res.: Atmos. 117 (D13) https://doi.org/10.1029/2012JD017730.

Jorba, O., Pandolfi, M., Spada, M., Baldasano, J., Pey, J., Alastuey, A., Arnold, D., Sicard, M., Artiñano, B., Revuelta, M., Querol, X., 2013. Overview of the meteorology and transport patterns during the DAURE field campaign and their impact to PM observations. Atmos. Environ. 77, 607–620. https://doi.org/10.1016/j.atmosenv.2013.05.040. URL https://www.sciencedirect.com/science/article/pii/S1352231013003890.

Kaiser, J., Heil, A., Andreae, M., Benedetti, A., Chubarova, N., Jones, L., Morcrette, J.-J., Razinger, M., Schultz, M., Suttie, M., et al., 2012. Biomass burning emissions estimated with a global fire assimilation system based on observed fire radiative power. Biogeosciences 9, 527–554.

Karanasiou, A., Panteliadis, P., Pérez, N., Minguillón, M.C., Pandolfi, M., Titos, G., Viana, M., Moreno, T., Querol, X., Alastuey, A., 2020. Evaluation of the Semi-Continuous OCEC analyzer performance with the EUSAAR2 protocol. Sci. Total Environ. 747, 141 266.

Kennedy, I.M., 2007. The health effects of combustion-generated aerosols. Proc. Combust. Inst. 31, 2757–2770.

Klimont, Z., Kupiainen, K., Heyes, C., Purohit, P., Cofala, J., Rafaj, P., Borken-Kleefeld, J., Schöpp, W., 2017. Global anthropogenic emissions of particulate matter including black carbon. Atmos. Chem. Phys. 17, 8681–8723.

Klose, M., Jorba, O., Gonçalves Ageitos, M., Escribano, J., Dawson, M.L., Obiso, V., Di Tomaso, E., Basart, S., Montané Pinto, G., Macchia, F., et al., 2021. Mineral dust cycle in the Multiscale Online Nonhydrostatic AtmospheRe CHemistry model (MONARCH) version 2.0. Geoscient. Model Develop. 14, 6403–6444.

Kuenen, J., Visschedijk, A., Jozwicka, M., Denier Van Der Gon, H., 2014. TNO-MACC_II emission inventory; a multi-year (2003–2009) consistent high-resolution European emission inventory for air quality modelling. Atmos. Chem. Phys. 14, 10 963–10 976.

Kuenen, J., Dellaert, S., Visschedijk, A., Jalkanen, J.-P., Super, I., Denier van der Gon, H., 2022. CAMS-REG-v4: a state-of-the-art high-resolution European emission inventory for air quality modelling. Earth Syst. Sci. Data 14, 491–515.

Lana, A., Bell, T.G., Simó, R., Vallina, S.M., Ballabrera-Poy, J., Kettle, A.J., Dachs, J., Bopp, L., Saltzman, E.S., Stefels, J., Johnson, J.E., Liss, P.S., 2011. An updated climatology of surface dimethlysulfide concentrations and emission fluxes in the global ocean. Global Biogeochem. Cycles 25. https://doi.org/10.1029/2010GB003850. URL https://agupubs.onlinelibrary.wiley.com/doi/abs/10.1029/2010GB003850.

López-Aparicio, S., Guevara, M., Thunis, P., Cuvelier, K., Tarrasón, L., 2017. Assessment of discrepancies between bottom-up and regional emission inventories in Norwegian urban areas. Atmos. Environ. 154, 285–296.

Manubens-Gil, D., Vegas-Regidor, J., Matthews, D., Shin, M., 2016. Assesment report on autosubmit, cylc and ecflow. Technical report.

Meroni, A., Pirovano, G., Gilardoni, S., Lonati, G., Colombi, C., Gianelle, V., Paglione, M., Poluzzi, V., Riva, G., Toppetti, A., 2017. Investigating the role of chemical and physical processes on organic aerosol modelling with CAMx in the Po Valley during a winter episode. Atmos. Environ. 171, 126–142.

Metzger, S., Dentener, F., Pandis, S., Lelieveld, J., 2002. Gas/aerosol partitioning: 1. A computationally efficient model. J. Geophys. Res.: Atmos. 107. ACH–16.

Minguillón, M.C., Perron, N., Querol, X., Szidat, S., Fahrni, S.M., Alastuey, A., Jimenez, J. L., Mohr, C., Ortega, A.M., Day, D., et al., 2011. Fossil versus contemporary sources of fine elemental and organic carbonaceous particulate matter during the DAURE campaign in Northeast Spain. Atmos. Chem. Phys. 11, 12 067–12 084.

Moreno-Ríos, A.L., Tejeda-Benítez, L.P., Bustillo-Lecompte, C.F., 2022. Sources, characteristics, toxicity, and control of ultrafine particles: An overview. Geosci. Front. 13, 101 147.

Morino, Y., Chatani, S., Tanabe, K., Fujitani, Y., Morikawa, T., Takahashi, K., Sato, K., Sugata, S., 2018. Contributions of condensable particulate matter to atmospheric organic aerosol over Japan. Environ. Sci. Technol. 52, 8456–8466.

Müller, T., Henzing, J., De Leeuw, G., Wiedensohler, A., Alastuey, A., Angelov, H., Bizjak, M., Collaud Coen, M., Engström, J., Gruening, C., et al., 2011. Characterization and intercomparison of aerosol absorption photometers: result of two intercomparison workshops. Atmos. Measur. Tech. 4, 245–268.

Ng, N., Canagaratna, M.R., Zhang, Q., Jimenez, J.L., Tian, J., Ulbrich, I.M., Kroll, J.H., Docherty, K.S., Chhabra, P.S., Bahreini, R., Murphy, S.M., Seinfeld, J.H., Hildebrandt, L., Donahue, N.M., DeCarlo, P.F., Lanz, V.A., Prevot, A.S.H., Dinar, E., Rudich, Y., Worsnop, D.R., 2010. Organic aerosol components observed in Northern Hemispheric datasets from Aerosol Mass Spectrometry. Atmos. Chem. Phys. 10 (10), 4625–4641. https://doi.org/10.5194/acp-10-4625-2010.

Nielsen, O.-K., 2013. EMEP/EEA air pollutant emission inventory guidebook 2013. Technical guidance to prepare national emission inventories. http://www.eea.europa.eu/publications/emep-eea-guidebook-2013.

Nussbaumer, T., Czasch, C., Klippel, N., Johansson, L., Tullin, C., 2008. Particulate emissions from biomass combustion in IEA countries, Survey on Measurements and Emission Factors. International Energy Agency (IEA) Bioenergy Task 32.

Ohlwein, S., Kappeler, R., Kutlar Joss, M., Künzli, N., Hoffmann, B., 2019. Health effects of ultrafine particles: a systematic literature review update of epidemiological evidence. Int. J. Public Health 64, 547–559.

Pai, S.J., Heald, C.L., Pierce, J.R., Farina, S.C., Marais, E.A., Jimenez, J.L., Campuzano-Jost, P., Nault, B.A., Middlebrook, A.M., Coe, H., Shilling, J.E., Bahreini, R., Dingle, J.H., Vu, K., 2020. An evaluation of global organic aerosol schemes using airborne observations. Atmos. Chem. Phys. 20 (5), 2637–2665. https://doi.org/10.5194/acp-20-2637-2020.

Pandolfi, M., Cusack, M., Alastuey, A., Querol, X., 2011. Variability of aerosol optical properties in the Western Mediterranean Basin. Atmos. Chem. Phys. 11, 8189–8203.

Pandolfi, M., Querol, X., Alastuey, A., Jimenez, J., Jorba, O., Day, D., Ortega, A., Cubison, M., Comerón, A., Sicard, M., et al., 2014. Effects of sources and meteorology on particulate matter in the Western Mediterranean Basin: An overview of the DAURE campaign. J. Geophys. Res.: Atmos. 119, 4978–5010.

Pandolfi, M., Ripoll, A., Querol, X., Alastuey, A., 2014. Climatology of aerosol optical properties and black carbon mass absorption cross section at a remote high-altitude site in the western Mediterranean Basin. Atmos. Chem. Phys. 14, 6443–6460.

Pandolfi, M., Alastuey, A., Pérez, N., Reche, C., Castro, I., Shatalov, V., Querol, X., 2016. Trends analysis of PM source contributions and chemical tracers in NE Spain during 2004–2014: a multi-exponential approach. Atmos. Chem. Phys. 16 (18), 11787–11805. https://doi.org/10.5194/acp-16-11787-2016.

Paunu, V.-V., Karvosenoja, N., Segersson, D., López-Aparicio, S., Nielsen, O.-K., Plejdrup, M.S., Thorsteinsson, T., Niemi, J.V., Vo, D.T., van der Gon, H.A.D., et al., 2021. Spatial distribution of residential wood combustion emissions in the Nordic countries: How well national inventories represent local emissions? Atmos. Environ. 264, 118 712.

Pérez, C., Haustein, K., Jorba Casellas, O., Janjic, Z., Huneeus, N., Baldasano Recio, J.M., Black, T., Basart, S., Nickovic, S., Miller, R., Perlwitz, J.P., Schulz, M., Thomson, M., 2011. Atmospheric dust modeling from meso to global scales with the online NMMB/BSC-Dust model – Part 1: Model description, annual simulations and evaluation. Atmos. Chem. Phys. 11 (24), 13001–13027. https://doi.org/10.5194/acp-11-13001-2011.

Pérez, N., Pey, J., Castillo, S., Viana, M., Alastuey, A., Querol, X., 2008. Interpretation of the variability of levels of regional background aerosols in the Western Mediterranean. Sci. Total Environ. 407, 527–540.

Petzold, A., Schönlinner, M., 2004. Multi-angle absorption photometry—a new method for the measurement of aerosol light absorption and atmospheric black carbon. J. Aerosol Sci. 35, 421–441.

Petzold, A., Schloesser, H., Sheridan, P.J., Arnott, W.P., Ogren, J.A., Virkkula, A., 2005. Evaluation of multiangle absorption photometry for measuring aerosol light absorption. Aerosol Sci. Technol. 39, 40–51.

Pey, J., Pérez, N., Castillo, S., Viana, M., Moreno, T., Pandolfi, M., López-Sebastián, J., Alastuey, A., Querol, X., 2009. Geochemistry of regional background aerosols in the Western Mediterranean. Atmos. Res. 94, 422–435.

Pey, J., Querol, X., Alastuey, A., Forastiere, F., Stafoggia, M., 2013. African dust outbreaks over the Mediterranean Basin during 2001–2011: PM 10 concentrations, phenomenology and trends, and its relation with synoptic and mesoscale meteorology. Atmos. Chem. Phys. 13, 1395–1410.

Poloniecki, J.D., Atkinson, R.W., de Leon, A.P., Anderson, H.R., 1997. Daily time series for cardiovascular hospital admissions and previous day's air pollution in London, UK. Occup. Environ. Med. 54, 535–540.

Prank, M., Sofiev, M., Tsyro, S., Hendriks, C., Semeena, V., Vazhappilly Francis, X., Butler, T., Denier van der Gon, H., Friedrich, R., Hendricks, J., et al., 2016. Evaluation of the performance of four chemical transport models in predicting the aerosol chemical composition in Europe in 2005. Atmos. Chem. Phys. 16, 6041–6070.

Querol, X., Alastuey, A., Rodriguez, S., Plana, F., Ruiz, C.R., Cots, N., Massagué, G., Puig, O., 2001. PM10 and PM2. 5 source apportionment in the Barcelona Metropolitan area. Catalonia, Spain, Atmos. Environ. 35, 6407–6419.

Querol, X., Pey, J., Pandolfi, M., Alastuey, A., Cusack, M., Pérez, N., Moreno, T., Viana, M., Mihalopoulos, N., Kallos, G., et al., 2009. African dust contributions to mean ambient PM10 mass-levels across the Mediterranean Basin. Atmos. Environ. 43, 4266–4277.

Reche, C., Querol, X., Alastuey, A., Viana, M., Pey, J., Moreno, T., Rodríguez, S., González, Y., Fernández-Camacho, R., De la Rosa, J., et al., 2011. New considerations for PM, Black Carbon and particle number concentration for air quality monitoring across different European cities. Atmos. Chem. Phys. 11, 6207–6227.

Riemer, N., Vogel, H., Vogel, B., Schell, B., Ackermann, I., Kessler, C., Hass, H., 2003. Impact of the heterogeneous hydrolysis of N2O5 on chemistry and nitrate aerosol formation in the lower troposphere under photosmog conditions. J. Geophys. Res.: Atmos. 108 https://doi.org/10.1029/2002JD002436. URL https://agupubs.onlinelibrary.wiley.com/doi/abs/10.1029/2002JD002436.

Ripoll, A., Pey, J., Minguillón, M.C., Perez, N., Pandolfi, M., Querol, X., Alastuey, A., 2014. Three years of aerosol mass, black carbon and particle number concentrations at Montsec (southern Pyrenees, 1570 m asl). Atmos. Chem. Phys. 14, 4279–4295.

Ripoll, A., Minguillón, M.C., Pey, J., Jimenez, J.L., Day, D.A., Sosedova, Y., Canonaco, F., Prévôt, A.S., Querol, X., Alastuey, A., 2015. Long-term real-time chemical characterization of submicron aerosols at Montsec (southern Pyrenees, 1570 m asl). Atmos. Chem. Phys. 15, 2935–2951.

Rodrıguez, S., Querol, X., Alastuey, A., Kallos, G., Kakaliagou, O., 2001. Saharan dust contributions to PM10 and TSP levels in Southern and Eastern Spain. Atmos. Environ. 35, 2433–2447.

Rodriguez-Rey, D., Guevara, M., Linares, M.P., Casanovas, J., Salmerón, J., Soret, A., Jorba, O., Tena, C., García-Pando, C.P., 2021. A coupled macroscopic traffic and pollutant emission modelling system for Barcelona. Transport. Res. Part D: Transp. Environ. 92, 102 725.

Sandradewi, J., Prévôt, A.S., Szidat, S., Perron, N., Alfarra, M.R., Lanz, V.A., Weingartner, E., Baltensperger, U., 2008. Using aerosol light absorption measurements for the quantitative determination of wood burning and traffic emission contributions to particulate matter. Environ. Sci. Technol. 42, 3316–3323.

Sarwar, G., Simon, H., Bhave, P., Yarwood, G., 2012. Examining the impact of heterogeneous nitryl chloride production on air quality across the United States. Atmos. Chem. Phys. 12, 6455–6473.

Schwartz, J., 2000. Harvesting and long term exposure effects in the relation between air pollution and mortality. Am. J. Epidemiol. 151, 440–448.

Shrivastava, M., Cappa, C.D., Fan, J., Goldstein, A.H., Guenther, A.B., Jimenez, J.L., Kuang, C., Laskin, A., Martin, S.T., Ng, N.L., et al., 2017. Recent advances in understanding secondary organic aerosol: Implications for global climate forcing. Rev. Geophys. 55, 509–559.

Sicard, M., Jorba, O., Ho, J.J., Izquierdo, R., De Linares, C., Alarcón, M., Comerón, A., Belmonte, J., 2021. Measurement report: Characterization of the vertical distribution of airborne Pinus pollen in the atmosphere with lidar-derived profiles – a modeling case study in the region of Barcelona, NE Spain. Atmos. Chem. Phys. 21 (23), 17807–17832. https://doi.org/10.5194/acp-21-17807-2021 https://acp.copernicus.org/articles/21/17807/2021/.

Simpson, D., Fagerli, H., Colette, A., Denier van der Gon, H., et al., 2020. How should condensables be included in PM emission inventories reported to EMEPCLFTAP?. In: Technical Report MSC-W 4/2020, pp. 1–72. MSC-W.

Skjøth, C.A., Geels, C., Berge, H., Gyldenkærne, S., Fagerli, H., Ellermann, T., Frohn, L. M., Christensen, J., Hansen, K.M., Hansen, K., Hertel, O., 2011. Spatial and temporal variations in ammonia emissions – a freely accessible model code for Europe. Atmos. Chem. Phys. 11, 5221–5236. https://doi.org/10.5194/acp-11-5221-2011. URL https://acp.copernicus.org/articles/11/5221/2011/.

Soni, A., Mandariya, A.K., Rajeev, P., Izhar, S., Singh, G.K., Choudhary, V., Qadri, A.M., Gupta, A.D., Singh, A.K., Gupta, T., 2021. Multiple site ground-based evaluation of carbonaceous aerosol mass concentrations retrieved from CAMS and MERRA-2 over the Indo-Gangetic Plain. Environ. Sci.: Atmos. 1, 577–590.

Spada, M., 2015. Development and evaluation of an atmospheric aerosol module implemented within the NMMB/BSC-CTM. Ph.D. thesis. Universitat Politècnica de Catalunya.

Spada, M., Jorba, O., Pérez García-Pando, C., Janjic, Z., Baldasano, J., 2013. Modeling and evaluation of the global sea-salt aerosol distribution: sensitivity to size-resolved and sea-surface temperature dependent emission schemes. Atmos. Chem. Phys. 13, 11 735–11 755.

Port de Barcelona: Memoria anual 2018, https://www.portdebarcelona.cat/es/web/autoritat-portuaria/memoria-2018, [Online; accessed 15-September-2022], 2019.

Thunis, P., Crippa, M., Cuvelier, C., Guizzardi, D., de Meij, A., Oreggioni, G., Pisoni, E., 2021. Sensitivity of air quality modelling to different emission inventories: A case study over Europe. Atmos. Environ.: X 10, 100 111.

Tie, X., Wu, D., Brasseur, G., 2009. Lung cancer mortality and exposure to atmospheric aerosol particles in Guangzhou. China, Atmos. Environ. 43, 2375–2377.

Timmermans, R., van der Gon, H.D., Kuenen, J., Segers, A., Honoré, C., Perrussel, O., Builtjes, P., Schaap, M., 2013. Quantification of the urban air pollution increment and its dependency on the use of down-scaled and bottom-up city emission inventories. Urban Climate 6, 44–62.

Tolocka, M.P., Saul, T.D., Johnston, M.V., 2004. Reactive uptake of nitric acid into aqueous sodium chloride droplets using real-time single-particle mass spectrometry. J. Phys. Chem. A 108, 2659–2665.

Trombetti, M., Thunis, P., Bessagnet, B., Clappier, A., Couvidat, F., Guevara, M., Kuenen, J., López-Aparicio, S., 2018. Spatial inter-comparison of Top-down emission inventories in European urban areas. Atmos. Environ. 173, 142–156.

Validzic, D., 2017. Clean Energy for All Europeans-European Union's New Legislative Framework.

Via, M., Minguillón, M.C., Reche, C., Querol, X., Alastuey, A., 2021. Increase in secondary organic aerosol in an urban environment. Atmos. Chem. Phys. 21, 8323–8339.

WHO, 2018. Global reference list of 100 core health indicators (plus health-related SDGs), Tech. rep. World Health Organization, p. 2018.

Wild, O., Zhu, X., Prather, M.J., 2000. Fast-J: Accurate simulation of in-and below-cloud photolysis in tropospheric chemical models. J. Atmos. Chem. 37, 245–282.

Yarwood, G., Rao, S., Yocke, M., Whitten, G., 2005. Updates to the carbon bond chemical mechanism: CB05, Final report to the US EPA. RT-0400675 8, 13.

Yue, D., Zhang, Q., Zhang, J., Liu, W., Chen, L., Wang, M., Li, R., Qin, S., Song, X., Ji, Y., 2023. Diesel exhaust PM2. 5 greatly deteriorates fibrosis process in pre-existing pulmonary fibrosis via ferroptosis. Environ. Int. 171, 107 706.

Yus-Díez, J., Bernardoni, V., Močnik, G., Alastuey, A., Ciniglia, D., Ivančič, M., Querol, X., Perez, N., Reche, C., Rigler, M., et al., 2021. Determination of the multiple-scattering correction factor and its cross-sensitivity to scattering and wavelength dependence for different AE33 Aethalometer filter tapes: a multi-instrumental approach. Atmos. Meas. Tech. 14, 6335–6355.

Yus-Díez, J., Via, M., Alastuey, A., Karanasiou, A., Minguillón, M.C., Perez, N., Querol, X., Reche, C., Ivančič, M., Rigler, M., et al., 2022. Absorption enhancement of black carbon particles in a Mediterranean city and countryside: effect of particulate matter chemistry, ageing and trend analysis. Atmos. Chem. Phys. 22, 8439–8456.

Zanatta, M., Gysel, M., Bukowiecki, N., Müller, T., Weingartner, E., Areskoug, H., Fiebig, M., Yttri, K.E., Mihalopoulos, N., Kouvarakis, G., et al., 2016. A European aerosol phenomenology-5: Climatology of black carbon optical properties at 9 regional background sites across Europe. Atmos. Environ. 145, 346–364.

Zhang, Q., Beekmann, M., Drewnick, F., Freutel, F., Schneider, J., Crippa, M., Prevot, A. S., Baltensperger, U., Poulain, L., Wiedensohler, A., et al., 2013. Formation of organic aerosol in the Paris region during the MEGAPOLI summer campaign: evaluation of the volatility-basis-set approach within the CHIMERE model. Atmos. Chem. Phys. 13, 5767–5790.